Supporting Information for

Heterochromatin and RNAi act independently to ensure genome stability in Mucorales human fungal pathogens

María Isabel Navarro-Mendoza[a,1,2], Carlos Pérez-Arques[a,1,2], and Joseph Heitman[a,2]

[a]Department of Molecular Genetics and Microbiology, Duke University School of Medicine, NC 27710, USA

[1]Equally-contributing authors

[2]To whom correspondence may be addressed

To whom correspondence may be addressed: María Isabel Navarro-Mendoza (maribel.navarro@duke.edu), Carlos Pérez-Arques (carlos.parq@duke.edu), and Joseph Heitman (heitm001@duke.edu). 322 Research Drive, CARL Building, Box 3546. Durham, NC 27710. USA. Telephone: 919-684-2824

This PDF file includes:

Supporting information text

Extended Materials and Methods

Figures S1 to S10

Tables S1 to S4

Legends for datasets S1 to S4

SI References

Other supporting materials for this manuscript include the following:

Datasets S1 to S4

SI Appendix

Supporting information text

Extended Materials and Methods

Ortholog search and phylogenomic tree inference

Experimentally curated KMT, DNMT, KDM, and accessory proteins multi-FASTA datasets were used as queries for a PSI-BLAST v2.12.0 search (85) against a proteomic database comprised of 86 fungal species (86-119), knowingly intending to oversample Mucoromycota and fungal pathogen species but also selecting at least one representative of each fungal phylum if genomes were publicly available (see Dataset S1 for a comprehensive list of query protein sequences and species analyzed). PSI-BLAST searches were iterated for three consecutive runs, retrieving matches with E-values ≤ 0.001. Then, every match was subjected to a reciprocal BLASTp search against a database comprising the whole proteomes of the same species that were utilized as queries. From all of the initial matches, only those that satisfied a positive reciprocal BLASTp match were regarded as putative homologs (protein FASTA sequences are contained in Dataset S4). Non-reciprocal matches were examined manually to assess the efficacy of our strategy and correct any possible error in our workflows or protein databases. InterPro (IPR) protein domains from CDD, Gene3D, HAMAP, PANTHER, Pfam, PIRSF, PRINTS, PROSITE, SFLD, SMART, SUPERFAMILY, and TIGFRAM databases were predicted on those protein matches sequences deemed putative homologs using InterProScan v5.59-91.0 (120). Protein predicted domains and full-length sequences were plotted as rectangle diagrams for visual evaluation. Briefly, every database protein domain that matched the same IPR entry was collapsed to show only unique IPR domains, and these were color-coded, scaled, and plotted for every chromatin remodeler or accessory protein analyzed (see Dataset S2). Hierarchically redundant IPR entries, e.g., super-, sub- and families, were also collapsed, showing those that

bore the maximum number of hits in the datasets. Species were sorted according to phylogenies shown on Fig. 1 and *SI Appendix* Fig. S2 to facilitate visual evaluation, and those phylogenies were generated as follows. BUSCO v5.4.3 fungal OrthoDB v10 dataset “fungi_odb10” (121) was employed to conduct orthology searches in a subset of 65 species’ proteomes to avoid redundancy, selecting a total of 389 single-copy orthologs that were present in ≥ 90 % of the species and in *Rozella allomycis,* that was used as the outgroup for further phylogenetic analyses. Protein sequences of those single-copy orthologs in every species were aligned by MAFFT v7.475 (122), automatically selecting an appropriate alignment strategy, using the Smith-Waterman algorithm (--localpair) and a maximum of 1,000 iterations. Protein alignments were trimmed and gaps removed by TrimAl v1.4.rev15 (123) and the gappyout method, and trimmed alignments were utilized as partitions by IQ-TREE v2.2.0.3 (124) to infer a phylogenetic tree with 1,000 ultrafast bootstraps and SH-aLRT replicates, automatically detected best fitted protein substitution model, and setting *R. allomycis* as outgroup. In addition, 42108 was used as seed for reproducibility.

Repeats and transposable element prediction

Structural repeats and putative TEs were predicted by RepeatModeler2 v2.0.3 (125) allowing for LTR structural identification (-LTRstruct). This raw repeat library was merged with the RepBase database “RepBaseRepeatMaskerEdition-20181026” (126) to annotate every possible repeat in the genome using RepeatMasker v4.1.3 (http://www.repeatmasker.org/) slow search (-s), skipping bacterial insertion element check (-no_is). The subsequent GFF file was regarded as a raw structural repeat annotation file, but additional effort was directed to generating a curated TE library and annotation file. First, ORFs longer than 300 bp were predicted across the sequences contained in the RepeatModeler2 library using EMBOSS v6.6.0.0 getorf (127). Then, InterProScan was utilized to predict protein domains encoded by this ORFs. Each full-length element together with their ORFs and protein domain were scaled, color-coded, and plotted to

allow visual inspection as described above. Briefly, repeats encoding protein domains frequently associated with TE activity (e.g., reverse transcriptase, transposase, RNase, nucleic acid binding) were retained, and the domain type and relative position within each sequence was used to manually curate bona fide TE sequences, particularly the position of an Integrase-related protein domain before or after the reverse transcriptase and RNase tandem to discriminate between Ty1/Copia or Ty3/Gypsy LTR retrotransposons, respectively (128). Lastly, this curated TE library was used with RepeatMasker to annotate every TE copy with the same parameters as above, but also skipping simple repeats (-nolow), small RNA genes (-norna), and ensuring a stringent cut-off value of 5,000 (-cutoff 5000) to obtain mostly full-length elements to generate a curated TE annotation file.

ChIP and RNA isolation and sequencing

$2.5x10^7$ spores from each RNAi mutant and MU402 wild-type strains were cultured in 100 mL of YPD medium for 16 hours with constant shaking (250 rpm) at 26 ºC. Two biological replicates were harvested and processed for each sample. Samples were sonicated using a Bioruptor (Diogenode) with pulses of 30 s ON/OFF for 35 cycles to obtain a sheared chromatin of 100-300 bp, then they were divided for antibody IP and input DNA control. For ChIP samples, anti-Histone H3 (di methyl K9) ChIP Grade ab1220 (Abcam), anti-Histone H3 (tri methyl K9) ChIP Grade ab8898 (Abcam), and RNA pol II antibody 39497 (Active Motif) antibodies were used to immunoprecipitated the DNA. According to their isotypes, primary ChIP antibodies were conjugated to protein A or G magnetic beads before DNA purification. Samples were washed and de-cross-linked following a previously established procedure (40), and DNA was purified and eluted using a phenol:chloroform extraction method. IP and Input DNA samples were used to prepare libraries with Roche KAPA HyperPrep Kit, loaded into an Illumina NovaSeq 6000 S Prime flow cell and sequenced to obtain 100-bp paired-end reads. For total RNA purification, mycelial samples were purified with a miRNeasy Mini Kit (QIAGEN) following the procedure for total RNA

purification supplied by the manufacturer. The same total RNA sample was used to generate both small and long RNA libraries and subsequent sequencing, aiming to minimize biological differences between small and long RNA datasets from the same strain. Long RNA libraries were prepared by an rRNA removal method, using Illumina Stranded Total RNA Prep with Ribo-Zero Gold rRNA Removal Kit. This method allowed using customized *M. lusitanicus* 28S, 18S, and 5.8S rDNA probes, predicted by Barrnap v0.9. Libraries were loaded into an Illumina NovaSeq 6000 S Prime flow cell and sequenced for 150-bp paired-end reads. sRNA libraries were amplified using QIAseq miRNA library kit, loaded into a High-Output flow cell, and sequenced in an Illumina NextSeq 500 sequencing system to obtain 75-bp single-reads.

ChIP-seq data analysis

NovaSeq Control Software v1.7.5 generated one FASTQ dataset per flow-cell lane and sample that were concatenated if needed into a single dataset per sample. Dataset quality was assessed by FastQC v0.11.9 (https://www.bioinformatics.babraham.ac.uk/projects/fastqc/) and results were jointly evaluated after being processed by MultiQC v1.12 (129). Reads were processed by Trim Galore! v0.6.7 powered by Cutadapt v1.18 (130) to remove adapters, low quality reads (--quality 20), and reads shorter than 50 nt (--length 50). Processed reads were aligned using the BWA-MEM v.0.7.17 (arXiv:1303.3997) algorithm for medium and long reads to the *M. lusitanicus* MU402 genome (https://mycocosm.jgi.doe.gov/Muccir1_3/Muccir1_3.info.html), set at default parameters, and alignment files sorted with Samtools v1.3.1 (131). Coverage bigWig files for H3K9me2, -me3, and RNA pol II were generated from alignments using Deeptools2 v3.5.1 (132) bamCoverage for IP and Input DNA separately and bamCompare to assess the ratio IP/Input, normalizing using CPM and a binsize of 25 nucleotides. H3K9me2 and -me3 enrichment values in 10-kb windows across the whole genome were determined using Deeptools2 multiBigwigSummary. To identify broad enriched regions between each IP/Input pair of H3K9me2 or -me3, MACS2 v2.2.7.1 predictd (133) was used to predict fragment length, and

this value fed into callpeak, keeping duplicates and setting an effective genome size as precalculated by Kent's utils v438 faCount (134). Customized BED files containing genes (coding sequence including introns), repeated, and intergenic sequences were extracted from a publicly available GFF3 annotation file and the previously generated repeat file using BEDtools v2.27.1 utilities sort and complement (135). H3K9me2 and -me3 broad peaks in the wild-type strain were intersected using BEDtools intersect and the resulting overlapping H3K9me2/me3 peaks were mapped to gene, repeat, and intergenic features to calculate the number of H3K9me base pairs in each feature using BEDtools intersect and Bioawk v20110810 (https://github.com/lh3/bioawk/).

Long RNA-seq data analysis

Initial raw read processing was conducted as above, and processed reads were mapped to the genome using RNA-seq aligner STAR v.2.7.10a (136), ensuring all best scoring alignments were reported as primary alignments up to 500 alignments, and a predicted intron size ranging from 10 to 1000 bases. Alignments were sorted and classified into forward and reverse stranded by Samtools sort, view, and merge according to their flag values as follows: forward alignments included first-pair alignments from the reverse strand (-f 64 and 16) and second-pair alignments excluding those from the reverse strand (-f 128 and -F 16), and reverse alignments included second-pair alignments from the reverse strand (-f 128 and 16) and first-pair alignments excluding those from the reverse strand (-f 64 and -F 16). Then, bamCoverage bigWig files were generated as described above. Counts per transcript were quantified using featureCounts v2.0.1 (137) from the Subread package and a customized annotation file including gene annotation from JGI and the newly identified TEs. Briefly, primary alignments from read pairs were mapped to exon features in the annotation file, ignoring chimeric alignments, and assigning a fraction of counts in case of multimapping alignments or alignments overlapping two or more features to ensure transposable elements were properly quantified. In addition, strandedness was modified to forward or reverse strand as needed to generate sense or antisense counts, respectively. A count-

matrix containing all samples was utilized by the limma package v3.50.3 (138) to determine counts per million (CPM) values across genes and TEs, normalizing values by the trimmed mean of M-values (TMM) method. Log_2 fold change values were determined and a False Discovery Rate (FDR) test corrected by the Benjamini-Hochberg method was performed in pairwise sample comparisons across all genes and TEs.

sRNA-seq data analysis

Initial raw read processing was conducted as above, with some exceptions. NextSeq Control Software v4.0.1.41 was used for base-calling. In addition, 12-base pair Unique Molecular Identifiers (UMIs) were detected and printed into each FASTQ sequence header by UMI-tools v1.1.2 (139), discarding QIAGEN 3'-adapters (5'-AACTGTAGGCACCATCAAT-3'). After that, reads were further processed by Trim Galore! to remove Illumina PCR 3'-adapters, short and low-quality reads (--length 10 --quality 20), with unusually low stringency parameters (--stringency 4) to avoid trimming real bases from the 3'-end which would bias the sRNA length analysis, i.e., adapter sequences at 3-end were removed only if 4 or more bases matched an adapter sequence. Default stringency parameters (--stringency 1) would trim the 3'-end if only 1 base matched an adapter sequence, resulting in a random 1-bp 3-trimming of ~25% reads. After that, processed reads were aligned to tRNA, rRNA, and whole genome sequences to generate quantitative statistics, concatenating replicates from the same strain and also, separately. In more detail, reads were aligned to the genome by Bowtie v1.3.1 (140), ensuring the best possible alignment and no mismatches (-v 0 --best). Then, aligned reads were deduplicated by UMI-tools to remove possible contaminants, tRNA and rRNA sequences were predicted using tRNAscan-SE v2.0.9 (141) and Barrnap v0.9 (https://github.com/tseemann/barrnap/), respectively. Reads were aligned separately to tRNA and rRNA sequences using identical parameters as above. All of these alignments were counted using Samtools v1.3.1 and Bioawk. Aligned reads mapping to the genome but not to tRNA or rRNA sequences were used for further analyses. Read length and the

presence of uracil/thymine as their first, 5'-nucleotide was assessed using Samtools and Bioawk. Aligned reads mapping to intronic, exonic, repeated, and intergenic features (see above) were counted using BEDtools coverage. Then, sRNA content across genes and transposable elements was quantified using ShortStack v3.8.5 (142) and a manually generated ShortStack annotation file comprising JGI gene annotation and our newly identified transposable elements. ShortStack realigned the reads allowing for multi-mapping alignment discovery, powered by Bowtie and reporting every possible alignment lacking mismatches (in short, ShortStack parameters --mismatches 0 --bowtie_m 'all'; that result in Bowtie parameters -v 0 -a). Multi-mapping alignments were placed as a fraction of all mapped reads (--mmap f), and siRNA predicted sizes were set to 21-25 nucleotides (--dicermin 21 --dicermax 25). bamCoverage files were generated as described above.

Data statistical analyses and visualization

Cartesian, two-dimensional graphs were plotted using R ggplot2 v3.3.6 (143) and ggpubr v0.4.0 (https://github.com/kassambara/ggpubr/) packages. One-way ANOVA and Tukey's Honestly Significant Difference (HSD) testing was performed using the aov and TukeyHSD functions, respectively, and pairwise comparisons summarized in a compacted letter display employing the multcomp v1.4-20 package (144). Pearson's correlation coefficients and their assigned *p*-values, regression linear models, were computed and plotted using the ggpubr stat_cor function, and regression linear models with ggplot2 geom_smooth function. Genomic plots including ChIP enrichment, sRNA, and mRNA coverage and genomic feature data were rendered by Deeptools2 pyGenomeTracks v3.7 (145) utilizing customized configuration files, coverage files, and a BED12 annotation file comprising gene, repeated, and transposable element features. ChIP enrichment heatmaps across full-length sequences were plotted by Deeptools2 plotHeatmap, as well as enrichment profiles using plotProfile to display average values as the mean and standard deviation. Small and long RNA normalized or $\log_2$ fold change heatmaps were

plotted using the pheatmap package v1.0-12 (https://github.com/raivokolde/pheatmap/). Single-copy ortholog inferred phylogenomic trees were plotted by the ape v5.6-2 package (146), rotating branches and pruning leaves for visual effects, and using true branch lengths.

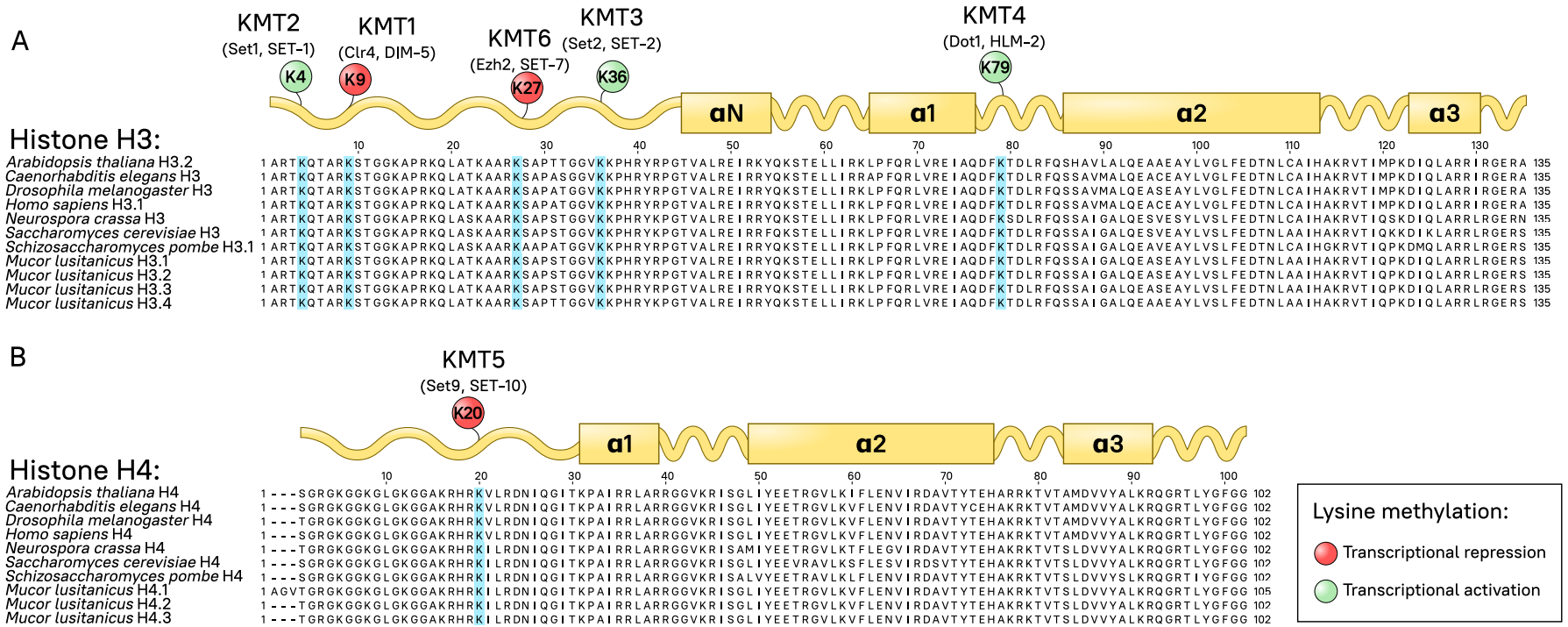

Fig. S1. *Mucor* histones display conserved residues for histone-lysine methyltransferase (KMT) activity. Histone H3 **(A)** and H4 **(B)** protein sequence alignment of several model organisms and *M. lusitanicus* is shown. Key lysine residues are highlighted in the alignment (cyan). Methyltransferases involved in histone-lysine methylation and the residue they target are depicted in a schematic representation of each histone protein, showing the N-terminal tail and the histone fold domain comprised of several α-helices (rectangles). Transcriptional repressive (red) and activating (green) modifications are displayed.

Fig. S2. Mucoromycota and other early-diverging fungi harbor an N-terminal chromodomain in Clr4. **(A)** Genomic plot of the *clr4* locus in *M. lusitanicus* MU402. Three different *clr4* gene models are shown (red arrowed blocks, dark gray for UTR regions), including the last reannotation according to our transcriptomic data. Position of Clr4 protein domains encoded in the DNA sequence is shown below gene models for reference. Sense transcripts are plotted as normalized $\log_2$ counts per million (CPM) values (green). **(B)** Clr4 methyltransferases of 60 fungal species clustered by phylogenomic relationship (left, tree), color-coded by different fungal phyla. The full-length, scaled protein sequence is shown along its predicted protein domains (legend). Chromodomain loss is pointed as a red circle in the phylogenomic tree. Phylogenomic distance (black solid line) is shown as changes per amino acid.

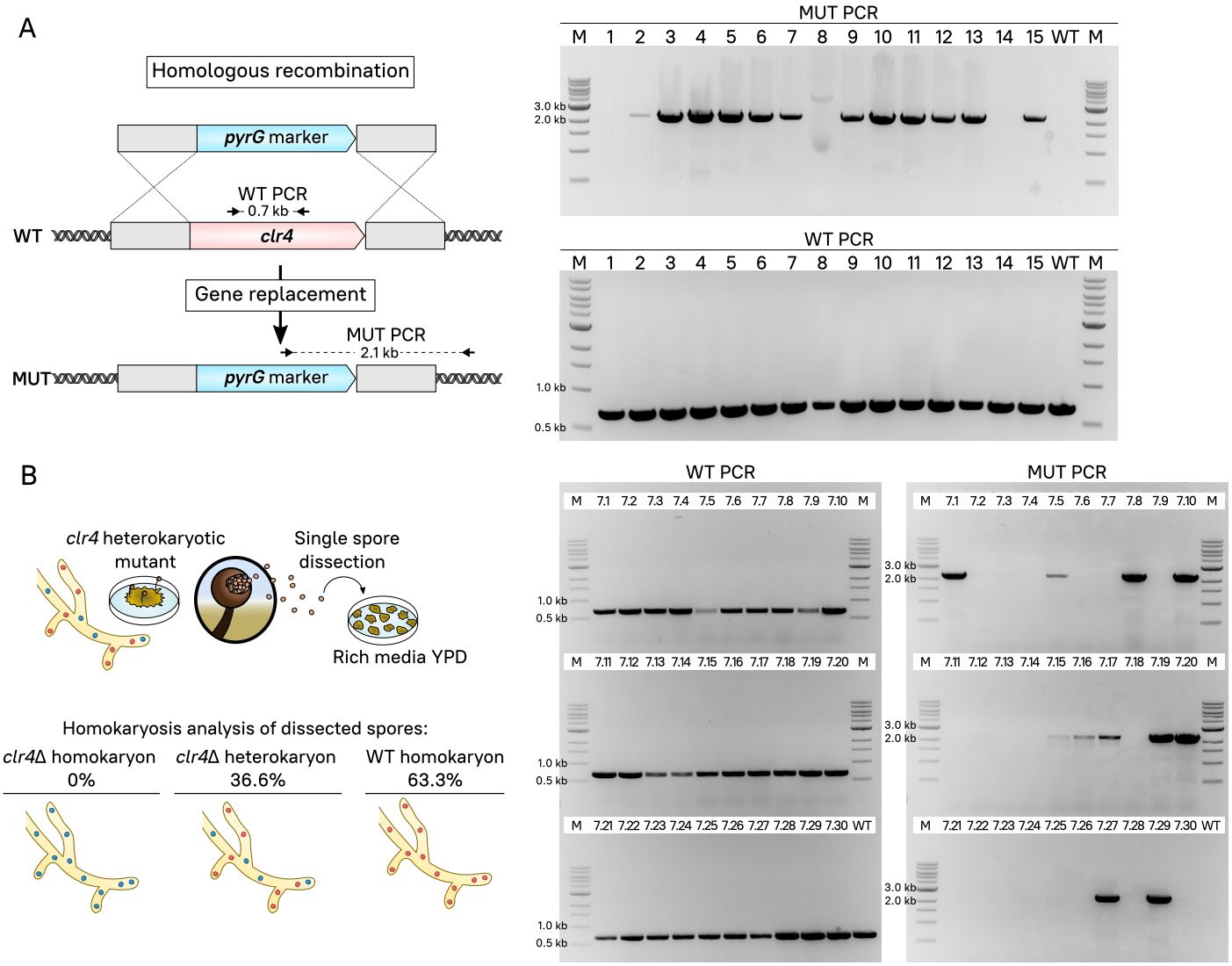

Fig. S3. *clr4* homokaryotic deletion results in lethality. **(A)** Schematic strategy followed for *clr4* gene deletion, replacing it with the *pyrG* marker. Primer binding sites for wild-type allele (WT PCR) and 3' mutant allele junction (MUT PCR) are shown. Gel electrophoresis showing PCR products from WT and MUT PCR in 15 transformants (1-15) and wild-type strain (WT). **(B)** Procedure to obtain homokaryotic mutants by single spore dissection from the heterokaryotic mutant #7. WT and MUT PCRs of 30 dissected spores (from 7.1 to 7.30). Spore genotype (mutant homokaryon, heterokaryon, and wild-type homokaryon) is summarized as percentage of total spores. M indicates DNA ladder in electrophoresis gels.

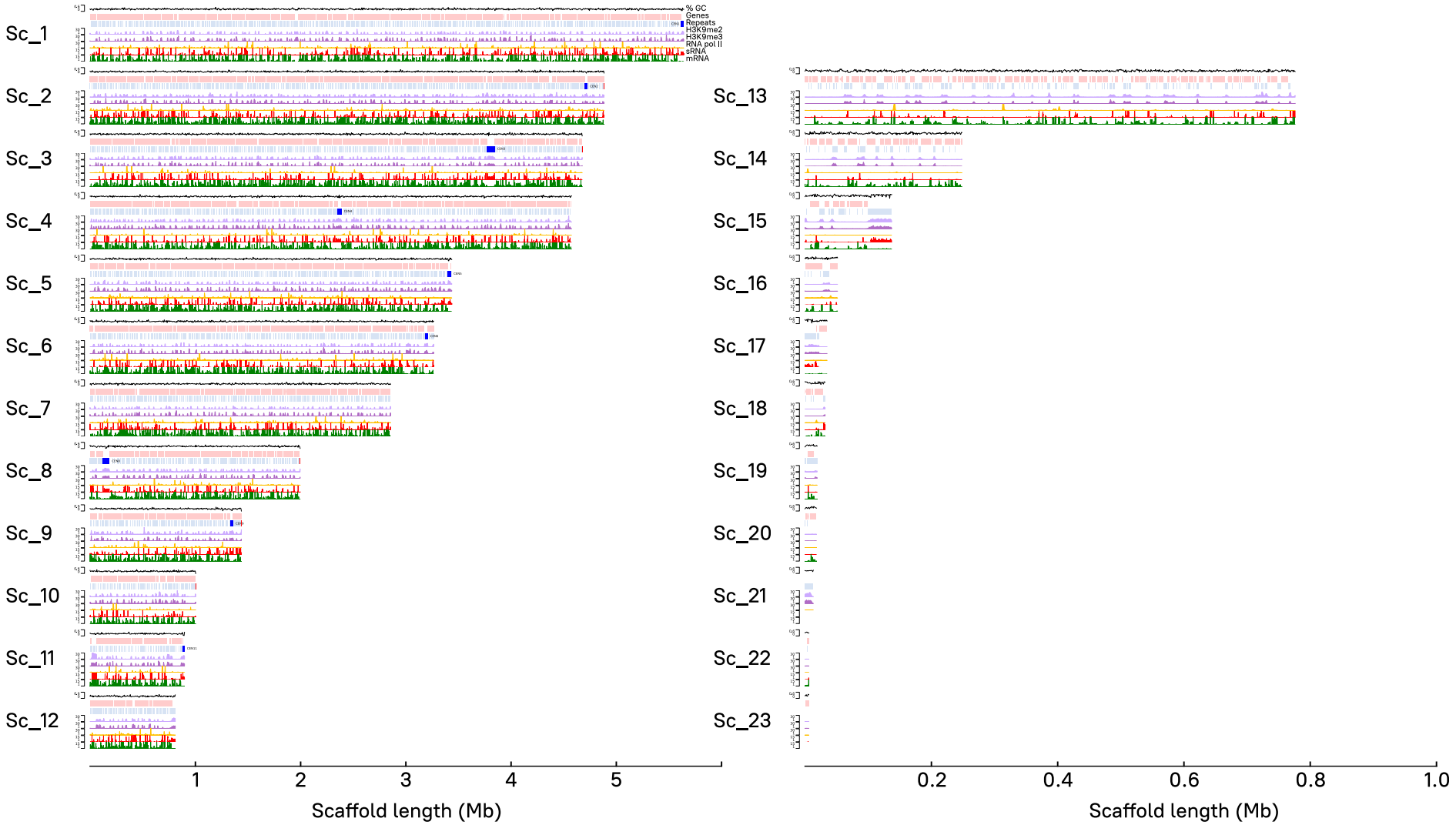

Fig. S4. H3K9me2, -me3, RNA pol II, sRNA, and mRNA genome-wide distribution in *M. lusitanicus*. Read coverage normalized as $\log_2$ CPM is shown as immunoprecipitated (IP) DNA/Input DNA ratio for H3K9me2 (light purple) and -me3 (purple) and RNA polymerase II (RNA pol II, gold); messenger RNA (mRNA, green) and sRNA (red) coverage as $\log_2$ CPM. Genes (light red) and repeated sequences (light blue) including pericentric regions (bright blue) are displayed, as well as GC content coverage as a percentage (black line). Every scaffold (1-23) and its length are plotted, but note that larger scaffolds comprising ≥ 95 % of the genome (1-12, left) are scaled differently than shorter scaffolds (13-23, right).

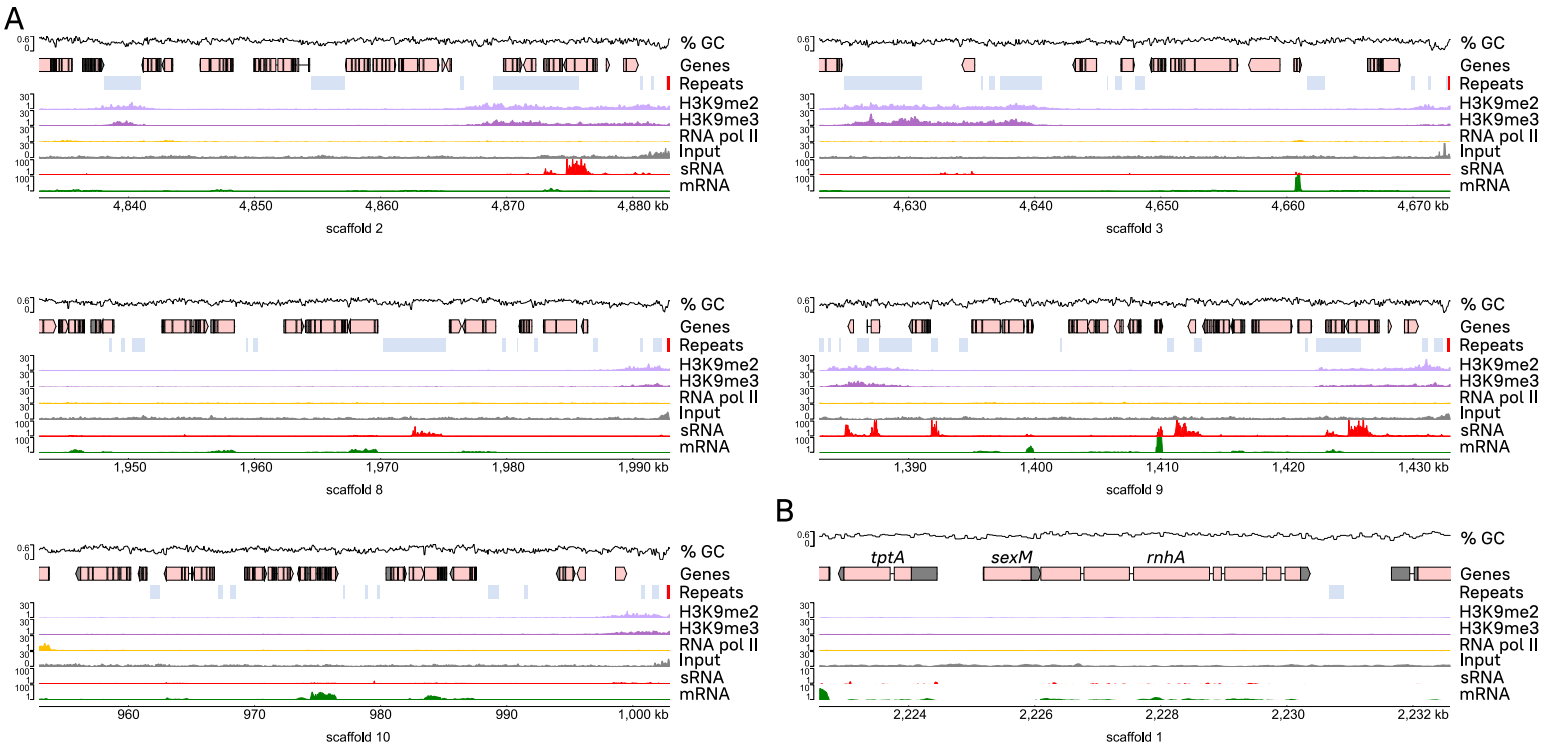

Fig. S5. H3K9me and sRNA enrichment in telomeric and sex-determining regions. H3K9me2 (light purple), -me3 (dark purple), and RNA polymerase II (RNA pol II, gold) IP/Input ratio, as well as Input control coverage for reference, are shown across 50-kb telomeric regions identified **(A)** and the *sex* locus **(B)**, and normalized as previously described. Transcripts (mRNA, green) and sRNA (red) coverages are also depicted. Genes (light red) and repeated sequences (light blue) including telomeric repeats (bright red) are displayed, as well as GC content coverage as a percentage.

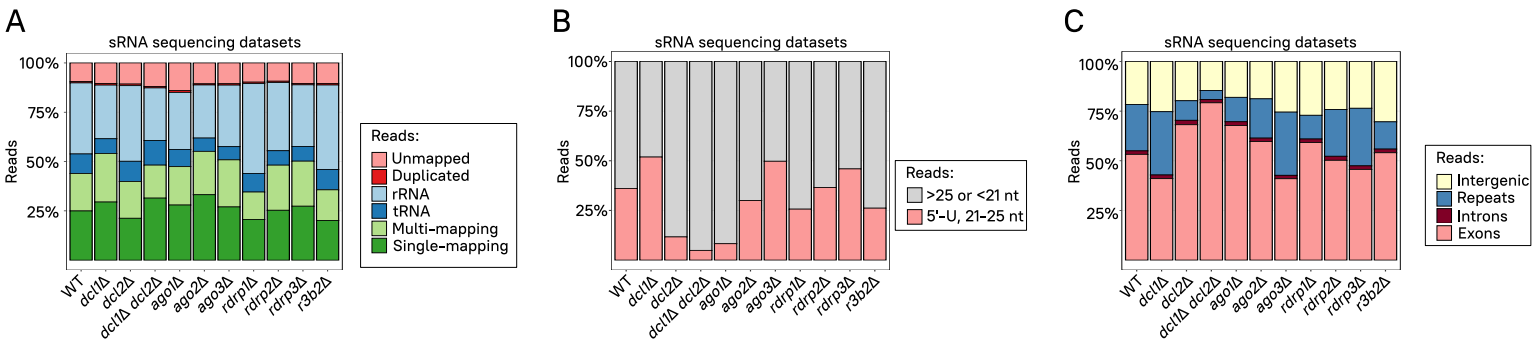

Fig. S6. Canonical sRNAs targeting primarily exonic sequences are generated by Dicer and Argonaute activity. **(A)** The percentage of unmapped, duplicated, rRNA or tRNA mapping, multi- or single-mapping reads to the genome in RNAi mutant and wild-type strain sRNA samples is depicted. **(B)** The percentage of aligned reads with a size ranging from 21 to 25 and bearing a 5'-uracil in the same samples is shown. **(C)** The percentage of aligned reads mapping to intergenic, repeated, intronic, and exonic features in the same samples is plotted.

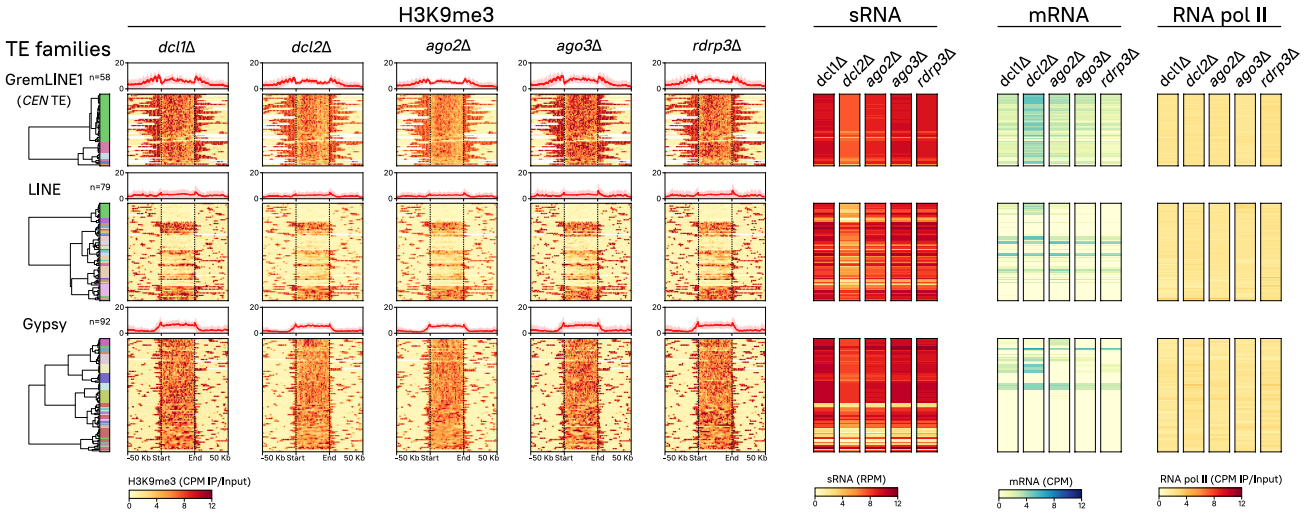

Fig. S7. H3K9me3, sRNA, mRNA, and RNA pol II enrichment across RNA transposons in non-essential RNAi paralog mutants. GremLINE1, other LINE, and Gypsy RNA transposon copies are clustered as in Fig. 3. Heatmaps depicting H3K9me3, sRNA, mRNA, and RNA polymerase II values in the wildtype and mutants in non-essential RNAi enzymes are plotted. H3K9me3 enrichment values are shown as IP/input DNA ratio of normalized $\log_2$ CPM from start to end of each copy (divided in 250 bins) and 50 kb upstream and downstream; as well as the mean value of all the copies in each family shown in a profile plot on top of each heatmap. sRNA and mRNA values are normalized to $\log_2$ reads per million (RPM) and CPM, respectively. RNA pol II enrichment values are also displayed as IP/Input ratio of normalized $\log_2$ CPM.

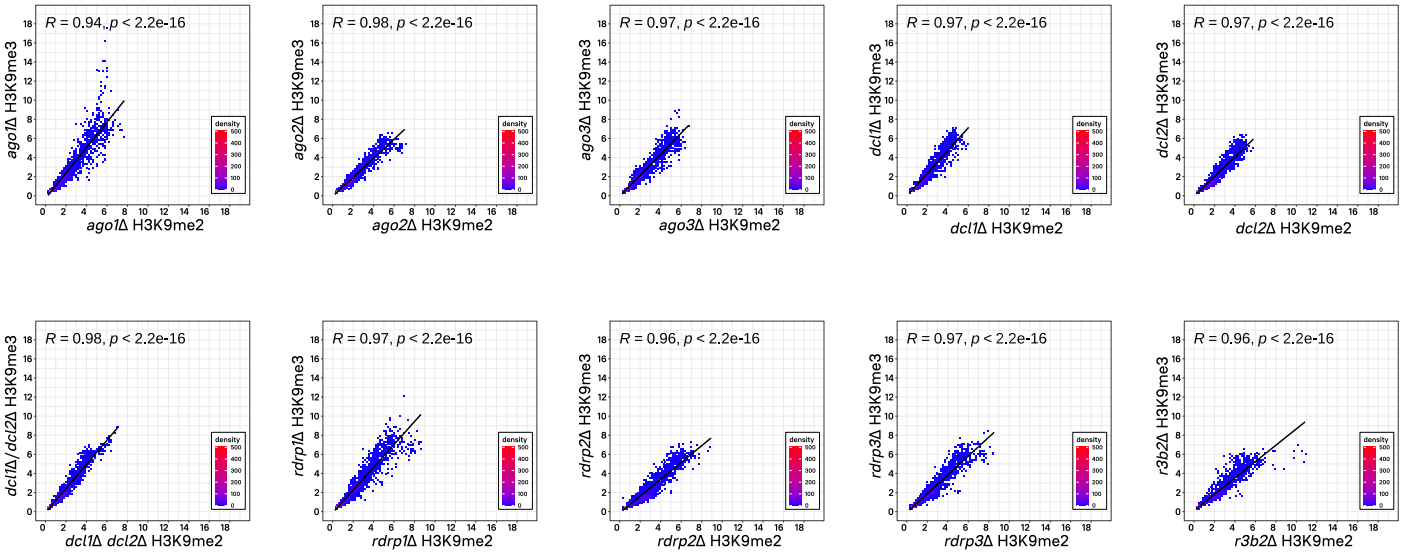

Fig. S8. H3K9me2 and -me3 distribution is significantly correlated in RNAi-deficient mutants. Pearson's correlation coefficient (R, dark line) and its *p*-value shown in a dot plot of H3K9me3 (y-axis) and -me2 (x-axis) average $\log_2$ CPM enrichment values in 10-kb regions representing the whole genome of *M. lusitanicus*. Overlapping dots are shown as blue-to-red colored corresponding to plotting density.

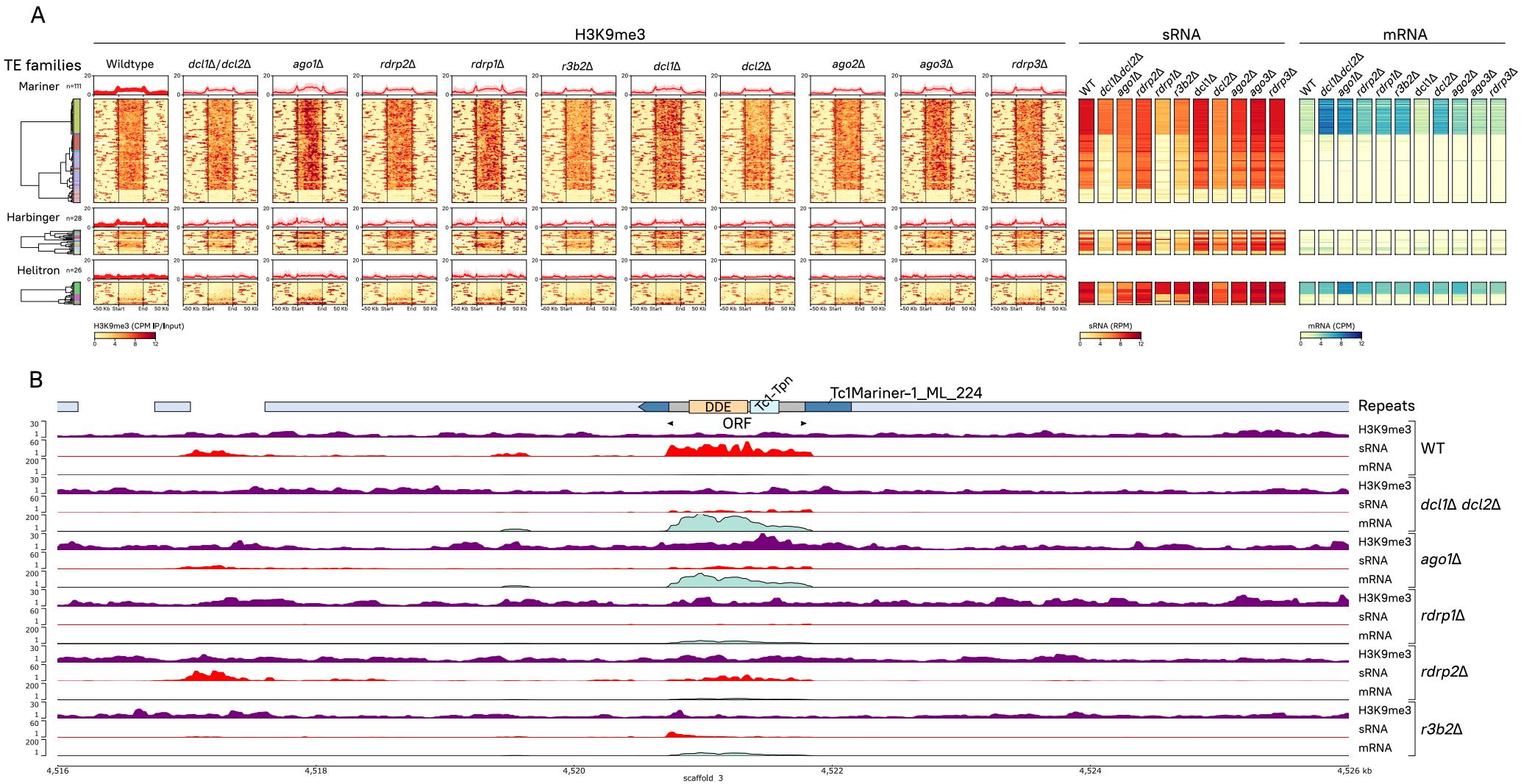

Fig. S9. DNA transposons are also targeted by both RNAi and H3K9me-based heterochromatin. **(A)** Every copy of Tc1/Mariner (n=111), PIF/Harbinger LINE (n=28), and RC/Helitron (n=26) DNA or Class II transposons identified in the genome are clustered according to their subfamily, H3K9me3, sRNA, and mRNA values in the wild-type *M. lusitanicus* strain. Heatmaps depicting H3K9me3, sRNA, mRNA, and RNA polymerase II values in wild-type and all RNAi mutant strains –essential and non-essential for RNAi– are plotted (see plot name above). As in Fig. 3, each row represents a single DNA transposon copy, and data values are aligned across all heatmaps to facilitate comparison. From left to right, a color-coded dendrogram indicating each element subfamily. Next, H3K9me3 enrichment values are shown as IP/input ratio of $\log_2$ CPM, from the start to the end of each copy and 50-kb upstream and downstream regions. The average of all the copies in each family is plotted in an H3K9me3 profile on top of each heatmap (bold red line shows the average and faded red background shows the standard deviation). Next heatmap to the right shows sRNA values normalized to $\log_2$ RPM, followed by a sense transcript heatmap (mRNA) in $\log_2$ CPM. The last heatmap on the right depicts RNA pol II enrichment values as IP/Input ratio of $\log_2$ CPM. **(B)** Tc1/Mariner-1 (blue arrowed block) representative genomic plot showing H3K9me3, sRNA, and mRNA data normalized as in **(A)** for canonical (*dcl1*Δ *dcl2*Δ, *ago1*Δ, *rdrp2*Δ, and *rdrp1*Δ) and alternative (*rdrp1*Δ and *r3b2*Δ) RNAi-deficient mutants. Transposition-related protein domains (colored rectangles) encoded by Tc1/Mariner-1_ML_224 ORF sequence (gray rectangle) and their position is shown. Other structural repeats (light blue rectangles) are plotted for reference.

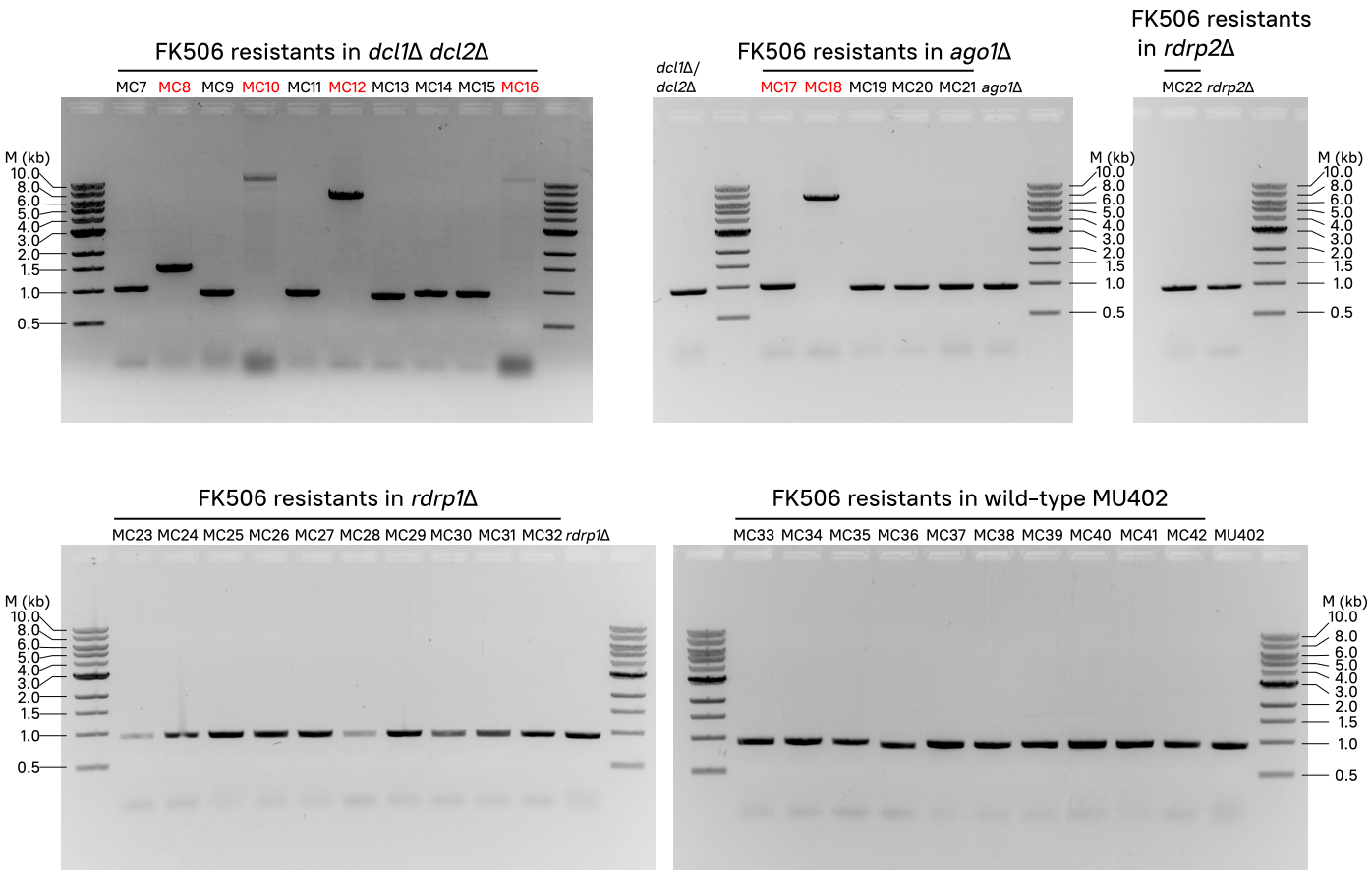

Fig. S10. Loss of canonical Dicer or Ago activities leads to large insertions and FK506 target disruption. The FKBP12-encoding *fkbA* locus was PCR-amplified in FK506-resistant isolates in different RNAi-deficient backgrounds (shown on top of each electrophoresis gel picture). *fkbA* sequences containing insertions (also confirmed by Sanger-sequencing) are highlighted in red, and were only found in *dcl1*Δ *dcl2*Δ and *ago1*Δ mutant strains. RNAi-deficient and wild-type strains not exposed to FK506 were also analyzed and included as FK506-sensitive controls. Lanes marked as M indicate DNA ladder and expected fragment sizes.

Table S1. Transposable elements identified in *M. lusitanicus*[1]

Name	Scaffold	Start	End	Strand
RChelitron-2_ML_1	scaffold_1	59075	64314	+
Tc1Mariner-2_ML_2	scaffold_1	506088	507741	+
Tc1Mariner-4_ML_3	scaffold_1	533090	534276	-
Gypsy-11_ML_4	scaffold_1	548786	550886	+
LINE-19_ML_5	scaffold_1	636962	638300	-
DIRS1-1_ML_6	scaffold_1	669754	671914	-
Tc1Mariner-2_ML_7	scaffold_1	680928	682581	-
Tc1Mariner-1_ML_8	scaffold_1	767427	769074	-
Tc1Mariner-2_ML_9	scaffold_1	900299	901952	+
PIFharbinger-2_ML_10	scaffold_1	1075426	1076217	+
PIFharbinger-10_ML_11	scaffold_1	1083344	1084188	+
RChelitron-1_ML_12	scaffold_1	1095022	1105954	+
LINE-11_ML_13	scaffold_1	1206459	1207551	-
LINE-6_ML_14	scaffold_1	1232677	1237995	+
LINE-7_ML_15	scaffold_1	1239265	1240306	-
LINE-11_ML_16	scaffold_1	1246524	1247309	-
Gypsy-1_ML_17	scaffold_1	1337965	1343514	-
LINE-8_ML_18	scaffold_1	1470621	1472646	+
Tc1Mariner-1_ML_19	scaffold_1	1476466	1478114	+
PIFharbinger-2_ML_20	scaffold_1	1642829	1643621	+
Gypsy-13_ML_21	scaffold_1	1712849	1715105	+
PIFharbinger-1_ML_22	scaffold_1	1813721	1816602	-
RChelitron-2_ML_23	scaffold_1	2145195	2150369	+
Tc1Mariner-2_ML_24	scaffold_1	2239161	2240812	+
LINE-3_ML_25	scaffold_1	2240968	2242011	-
PIFharbinger-3_ML_26	scaffold_1	2243268	2244195	+
LINE-3_ML_27	scaffold_1	2249852	2250558	-
Tc1Mariner-2_ML_28	scaffold_1	2250841	2252493	-
LINE-3_ML_29	scaffold_1	2252491	2257999	-
RChelitron-1_ML_30	scaffold_1	2409515	2415660	+
Gypsy-1_ML_31	scaffold_1	2443021	2448569	-
Gypsy-10_ML_32	scaffold_1	2450069	2450900	-
Tc1Mariner-1_ML_33	scaffold_1	2505397	2507045	+
Gypsy-14_ML_34	scaffold_1	2602990	2607776	-
PIFharbinger-1_ML_35	scaffold_1	2724893	2727772	-
LINE-9_ML_36	scaffold_1	2750807	2751366	+
LINE-11_ML_37	scaffold_1	2874519	2875619	+
Gypsy-9_ML_38	scaffold_1	3232247	3237336	-
PIFharbinger-1_ML_39	scaffold_1	3238966	3241846	+
Tc1Mariner-5_ML_40	scaffold_1	3327534	3329207	-
Gypsy-6_ML_41	scaffold_1	3333312	3334483	-
Tc1Mariner-1_ML_42	scaffold_1	3334961	3336609	+

Name	Scaffold	Start	End	Strand
Tc1Mariner-2_ML_43	scaffold_1	3338046	3339699	+
Tc1Mariner-2_ML_44	scaffold_1	3367481	3369134	+
Tc1Mariner-1_ML_45	scaffold_1	3450298	3451947	-
RChelitron-1_ML_46	scaffold_1	3550469	3556685	-
Tc1Mariner-1_ML_47	scaffold_1	3607135	3609115	-
Tc1Mariner-11_ML_48	scaffold_1	3847065	3847738	+
RChelitron-2_ML_49	scaffold_1	3855592	3860835	+
Tc1Mariner-3_ML_50	scaffold_1	3901016	3902677	-
Tc1Mariner-3_ML_51	scaffold_1	3944010	3945671	+
PIFharbinger-2_ML_52	scaffold_1	3953490	3954284	-
Tc1Mariner-3_ML_53	scaffold_1	3983408	3985070	-
Gypsy-15_ML_54	scaffold_1	4362330	4368330	+
Gypsy-15_ML_55	scaffold_1	4413846	4420198	-
Gypsy-2_ML_56	scaffold_1	4471178	4477260	-
Tc1Mariner-5_ML_57	scaffold_1	4477992	4479884	+
Tc1Mariner-2_ML_58	scaffold_1	4666907	4668560	+
Gypsy-2_ML_59	scaffold_1	4889828	4895911	+
RChelitron-1_ML_60	scaffold_1	4904164	4915041	-
LINE-L1-1_ML_61	scaffold_1	4974903	4977632	+
Tc1Mariner-1_ML_62	scaffold_1	4998772	5000420	-
LINE-6_ML_63	scaffold_1	5096344	5098227	-
DIRS1-2_ML_64	scaffold_1	5154541	5155087	-
PIFharbinger-2_ML_65	scaffold_1	5235549	5236343	+
Tc1Mariner-3_ML_66	scaffold_1	5317802	5319463	+
Tc1Mariner-3_ML_67	scaffold_1	5322967	5324628	-
Tc1Mariner-1_ML_68	scaffold_1	5475065	5476714	+
Gypsy-16_ML_69	scaffold_1	5504344	5505622	+
Tc1Mariner-3_ML_70	scaffold_1	5616002	5617663	-
PIFharbinger-4_ML_71	scaffold_1	5617617	5618148	-
GremLINE1-4_ML_72	scaffold_1	5621128	5622681	-
GremLINE1-1_ML_73	scaffold_1	5623342	5629299	+
GremLINE1-1_ML_74	scaffold_1	5629440	5635388	+
GremLINE1-1_ML_75	scaffold_1	5635389	5640055	+
Gypsy-4_ML_76	scaffold_10	0	5223	-
Tc1Mariner-1_ML_77	scaffold_10	260462	262111	+
LINE-14_ML_78	scaffold_10	288135	290462	+
Gypsy-1_ML_79	scaffold_10	320761	323377	+
Gypsy-10_ML_80	scaffold_10	715965	716818	+
Gypsy-17_ML_81	scaffold_10	722374	724472	-
Gypsy-4_ML_82	scaffold_10	726057	732172	+
LINE-19_ML_83	scaffold_10	794118	799540	-
Tc1Mariner-2_ML_84	scaffold_10	800066	801718	-
LINE-6_ML_85	scaffold_11	142409	143871	+

Name	Scaffold	Start	End	Strand
Tc1Mariner-4_ML_86	scaffold_11	439043	440333	-
Tc1Mariner-3_ML_87	scaffold_11	499857	501519	-
LINE-3_ML_88	scaffold_11	501932	507440	+
Tc1Mariner-6_ML_89	scaffold_11	552119	553213	-
Gypsy-2_ML_90	scaffold_11	872668	878748	+
GremLINE1-1_ML_91	scaffold_11	884717	885276	-
GremLINE1-1_ML_92	scaffold_11	885902	891861	+
GremLINE1-1_ML_93	scaffold_11	891941	897425	+
Gypsy-10_ML_94	scaffold_12	70333	71183	+
LINE-11_ML_95	scaffold_12	130570	131190	+
Gypsy-10_ML_96	scaffold_12	223130	223982	+
DIRS1-3_ML_97	scaffold_12	406677	408738	-
Tc1Mariner-6_ML_98	scaffold_12	494042	495098	+
Gypsy-18_ML_99	scaffold_12	561593	563744	-
Gypsy-19_ML_100	scaffold_12	565907	567095	+
LINE-9_ML_101	scaffold_12	759313	764708	+
GremLINE1-1_ML_102	scaffold_12	780213	786148	-
GremLINE1-1_ML_103	scaffold_12	786153	792098	-
GremLINE1-4_ML_104	scaffold_12	792097	798024	-
GremLINE1-4_ML_105	scaffold_12	798150	804078	-
GremLINE1-1_ML_106	scaffold_12	804204	809647	-
PIFharbinger-5_ML_107	scaffold_13	69983	71315	-
Gypsy-1_ML_108	scaffold_13	115801	121345	-
RChelitron-2_ML_109	scaffold_13	426726	431888	+
Tc1Mariner-1_ML_110	scaffold_13	506811	508460	+
RChelitron-4_ML_111	scaffold_13	576863	577709	+
PIFharbinger-6_ML_112	scaffold_13	577760	579284	+
LINE-L1-1_ML_113	scaffold_13	642983	644422	+
Tc1Mariner-2_ML_114	scaffold_15	25664	27317	-
GremLINE1-4_ML_115	scaffold_15	104067	109983	-
GremLINE1-1_ML_116	scaffold_15	109988	115956	-
GremLINE1-4_ML_117	scaffold_15	115977	121903	-
GremLINE1-1_ML_118	scaffold_15	122023	127963	-
GremLINE1-1_ML_119	scaffold_15	127962	133913	-
GremLINE1-2_ML_120	scaffold_15	133946	137282	-
Piggybac-1_Mcir_121	scaffold_16	33804	35019	+
LINE-16_ML_122	scaffold_17	0	4474	-
GremLINE1-1_ML_123	scaffold_17	4582	10517	-
GremLINE1-4_ML_124	scaffold_17	11176	12729	+
PIFharbinger-4_ML_125	scaffold_17	15709	16240	+
Tc1Mariner-3_ML_126	scaffold_17	16194	17855	+
GremLINE1-3_ML_127	scaffold_18	29067	31827	-
Gypsy-4_ML_128	scaffold_2	344999	351242	-

Name	Scaffold	Start	End	Strand
Gypsy-5_ML_129	scaffold_2	406710	412700	-
Gypsy-5_ML_130	scaffold_2	517655	523645	+
Tc1Mariner-3_ML_131	scaffold_2	639810	641480	+
LINE-11_ML_132	scaffold_2	725212	725916	+
Tc1Mariner-2_ML_133	scaffold_2	935659	937311	-
LINE-L1-1_ML_134	scaffold_2	1032990	1035596	-
LINE-10_ML_135	scaffold_2	1033400	1038935	-
RChelitron-1_ML_136	scaffold_2	1202553	1208001	+
RChelitron-2_ML_137	scaffold_2	1391435	1396610	-
Gypsy-4_ML_138	scaffold_2	1492129	1498180	+
Gypsy-3_ML_139	scaffold_2	1498772	1504699	+
Gypsy-6_ML_140	scaffold_2	1526998	1531557	-
LINE-11_ML_141	scaffold_2	1557397	1560142	+
Tc1Mariner-1_ML_142	scaffold_2	1561960	1563940	-
Gypsy-9_ML_143	scaffold_2	1674234	1675012	-
LINE-10_ML_144	scaffold_2	1701120	1702220	+
LINE-L1-1_ML_145	scaffold_2	1701125	1702832	+
Gypsy-20_ML_146	scaffold_2	1722870	1723542	-
Tc1Mariner-2_ML_147	scaffold_2	1790854	1792507	+
RChelitron-1_ML_148	scaffold_2	1859355	1870298	-
RChelitron-1_ML_149	scaffold_2	2110168	2116283	+
Tc1Mariner-3_ML_150	scaffold_2	2325951	2327611	-
Tc1Mariner-4_ML_151	scaffold_2	2430681	2432095	-
RChelitron-1_ML_152	scaffold_2	2489109	2490823	+
Tc1Mariner-1_ML_153	scaffold_2	2697135	2698782	-
Gypsy-10_ML_154	scaffold_2	2845958	2852009	+
Gypsy-6_ML_155	scaffold_2	3029085	3033644	-
LTR/Unknown-1_ML_156	scaffold_2	3168609	3170817	+
Gypsy-10_ML_157	scaffold_2	3443399	3449982	-
LINE-11_ML_158	scaffold_2	3575861	3577891	+
Gypsy-4_ML_159	scaffold_2	3758052	3764103	-
LINE-L1-1_ML_160	scaffold_2	3792266	3794144	+
LINE-10_ML_161	scaffold_2	4258762	4264208	+
LINE-L1-3_ML_162	scaffold_2	4264208	4264708	+
RChelitron-1_ML_163	scaffold_2	4289389	4295519	-
Piggybac-1_Mcir_164	scaffold_2	4314014	4315852	-
LINE-L1-1_ML_165	scaffold_2	4352316	4354834	-
Gypsy-3_ML_166	scaffold_2	4362188	4368115	+
Tc1Mariner-1_ML_167	scaffold_2	4381538	4383184	-
Tc1Mariner-3_ML_168	scaffold_2	4679027	4680689	-
GremLINE1-2_ML_169	scaffold_2	4707808	4713773	-
GremLINE1-2_ML_170	scaffold_2	4714562	4716735	+
Tc1Mariner-3_ML_171	scaffold_3	417685	419345	+

Name	Scaffold	Start	End	Strand
Gypsy-2_ML_172	scaffold_3	420421	426501	+
Tc1Mariner-2_ML_173	scaffold_3	502955	504608	-
LINE-19_ML_174	scaffold_3	679573	681107	+
LINE-L1-3_ML_175	scaffold_3	762959	768378	-
Tc1Mariner-1_ML_176	scaffold_3	768470	770117	-
DIRS1-4_ML_177	scaffold_3	773443	775369	+
PIFharbinger-3_ML_178	scaffold_3	776054	776981	+
LINE-6_ML_179	scaffold_3	939860	945178	-
Tc1Mariner-3_ML_180	scaffold_3	954500	956161	-
Tc1Mariner-3_ML_181	scaffold_3	959093	960754	+
Gypsy-5_ML_182	scaffold_3	989556	995546	-
Tc1Mariner-1_ML_183	scaffold_3	1019051	1021173	+
Copia_1_ML_184	scaffold_3	1106691	1108038	-
Tc1Mariner-1_ML_185	scaffold_3	1107973	1109621	+
LINE-13_ML_186	scaffold_3	1164914	1166593	+
LINE-9_ML_187	scaffold_3	1590619	1593886	+
LINE-10_ML_188	scaffold_3	1985187	1990634	+
LINE-L1-3_ML_189	scaffold_3	1990634	1991221	+
LINE-14_ML_190	scaffold_3	2301870	2305301	-
Tc1Mariner-2_ML_191	scaffold_3	2305763	2307418	-
Tc1Mariner-4_ML_192	scaffold_3	2381467	2382888	-
Gypsy-22_ML_193	scaffold_3	2391890	2397659	+
LINE-15_ML_194	scaffold_3	2470995	2476429	+
Tc1Mariner-1_ML_195	scaffold_3	2573625	2575271	+
LINE-11_ML_196	scaffold_3	2689286	2691082	-
Tc1Mariner-1_ML_197	scaffold_3	2836997	2838646	-
LINE-L1-1_ML_198	scaffold_3	2941233	2942449	-
Tc1Mariner-2_ML_199	scaffold_3	3155493	3157146	-
Gypsy-3_ML_200	scaffold_3	3277815	3283742	-
LINE-15_ML_201	scaffold_3	3302882	3307116	-
PIFharbinger-5_ML_202	scaffold_3	3641565	3642897	-
Tc1Mariner-3_ML_203	scaffold_3	3704235	3705896	+
GremLINE1-4_ML_204	scaffold_3	3776246	3782169	+
GremLINE1-1_ML_205	scaffold_3	3785060	3791025	+
GremLINE1-1_ML_206	scaffold_3	3791202	3797165	+
GremLINE1-1_ML_207	scaffold_3	3797164	3802935	+
GremLINE1-1_ML_208	scaffold_3	3802934	3808709	+
GremLINE1-1_ML_209	scaffold_3	3808709	3814476	+
GremLINE1-4_ML_210	scaffold_3	3814534	3820460	+
GremLINE1-1_ML_211	scaffold_3	3820464	3826333	+
GremLINE1-1_ML_212	scaffold_3	3826333	3832204	+
GremLINE1-1_ML_213	scaffold_3	3841429	3843599	-
Gypsy-23_ML_214	scaffold_3	4074669	4075740	-

Name	Scaffold	Start	End	Strand
Tc1Mariner-1_ML_215	scaffold_3	4121604	4123253	-
Tc1Mariner-3_ML_216	scaffold_3	4123962	4125621	-
LINE-10_ML_217	scaffold_3	4135453	4140881	+
LINE-L1-1_ML_218	scaffold_3	4138530	4141466	+
LINE-11_ML_219	scaffold_3	4264330	4265982	+
Tc1Mariner-4_ML_220	scaffold_3	4292552	4293974	-
PIFharbinger-7_ML_221	scaffold_3	4323022	4325285	+
PIFharbinger-5_ML_222	scaffold_3	4361511	4362843	+
LINE-19_ML_223	scaffold_3	4435732	4436380	-
Tc1Mariner-1_ML_224	scaffold_3	4520503	4522149	-
Tc1Mariner-9_ML_225	scaffold_4	54645	56694	-
Tc1Mariner-1_ML_226	scaffold_4	138792	140441	+
Tc1Mariner-4_ML_227	scaffold_4	930365	931779	+
Tc1Mariner-1_ML_228	scaffold_4	1078431	1080079	-
PIFharbinger-1_ML_229	scaffold_4	1150233	1153114	-
LTR/Unknown-2_ML_230	scaffold_4	1547088	1548120	-
Gypsy-4_ML_231	scaffold_4	1592443	1598494	-
Gypsy-10_ML_232	scaffold_4	1604518	1605370	-
DIRS1-5_ML_233	scaffold_4	1731081	1733187	-
LINE-9_ML_234	scaffold_4	1735810	1741203	-
Tc1Mariner-1_ML_235	scaffold_4	1801532	1803178	-
RChelitron-2_ML_236	scaffold_4	1820957	1826183	+
Tc1Mariner-1_ML_237	scaffold_4	1840378	1842024	-
Gypsy-24_ML_238	scaffold_4	1940329	1940881	+
LINE-3_ML_239	scaffold_4	2270490	2271238	-
LINE-3_ML_240	scaffold_4	2272906	2278414	-
PIFharbinger-8_ML_241	scaffold_4	2322835	2323405	-
LINE-3_ML_242	scaffold_4	2336014	2341523	+
LINE-3_ML_243	scaffold_4	2341803	2342610	+
LINE-3_ML_244	scaffold_4	2342607	2343521	+
GremLINE1-4_ML_245	scaffold_4	2351462	2357388	-
GremLINE1-3_ML_246	scaffold_4	2357389	2363323	-
GremLINE1-2_ML_247	scaffold_4	2363869	2369818	+
GremLINE1-4_ML_248	scaffold_4	2369818	2375739	+
GremLINE1-1_ML_249	scaffold_4	2375800	2381730	+
GremLINE1-5_ML_250	scaffold_4	2421133	2421982	-
Gypsy-5_ML_251	scaffold_4	2491357	2497347	-
PIFharbinger-9_ML_252	scaffold_4	2526978	2527863	+
PIFharbinger-10_ML_253	scaffold_4	2635220	2636744	-
RChelitron-1_ML_254	scaffold_4	2863402	2874253	-
Gypsy-25_ML_255	scaffold_4	2894620	2896228	-
PIFharbinger-1_ML_256	scaffold_4	2953056	2954339	+
Gypsy-5_ML_257	scaffold_4	3002155	3008145	-

Name	Scaffold	Start	End	Strand
Tc1Mariner-4_ML_258	scaffold_4	3291272	3292781	+
RChelitron-1_ML_259	scaffold_4	3547034	3553272	+
Gypsy-1_ML_260	scaffold_4	3900790	3902041	-
LINE-11_ML_261	scaffold_4	4154022	4155120	-
LINE-8_ML_262	scaffold_4	4172441	4174172	+
Tc1Mariner-2_ML_263	scaffold_4	4235272	4236924	+
Gypsy-6_ML_264	scaffold_4	4237192	4241752	-
LINE-19_ML_265	scaffold_4	4451684	4457131	-
Gypsy-4_ML_266	scaffold_4	4555284	4561335	-
Gypsy-6_ML_267	scaffold_5	84402	88961	+
RChelitron-2_ML_268	scaffold_5	250271	255502	-
Tc1Mariner-2_ML_269	scaffold_5	329309	330962	-
Gypsy-2_ML_270	scaffold_5	331799	337905	+
RChelitron-1_ML_271	scaffold_5	486386	491849	+
Tc1Mariner-4_ML_272	scaffold_5	512530	514039	-
Gypsy-5_ML_273	scaffold_5	563349	569339	-
Gypsy-7_ML_274	scaffold_5	1022147	1027234	+
Tc1Mariner-3_ML_275	scaffold_5	1372092	1373753	-
Tc1Mariner-3_ML_276	scaffold_5	1401187	1402848	-
LINE-11_ML_277	scaffold_5	1572568	1574059	+
Tc1Mariner-2_ML_278	scaffold_5	1742650	1744303	-
Tc1Mariner-1_ML_279	scaffold_5	1749689	1751334	-
Tc1Mariner-2_ML_280	scaffold_5	1858153	1859806	+
Gypsy-26_ML_281	scaffold_5	1860013	1862481	-
LINE-11_ML_282	scaffold_5	1866061	1868081	-
Gypsy-10_ML_283	scaffold_5	1913934	1914784	+
PIFharbinger-1_ML_284	scaffold_5	2107720	2110600	+
LINE-L1-1_ML_285	scaffold_5	2230378	2232693	+
LINE-11_ML_286	scaffold_5	2455584	2457909	+
Gypsy-8_ML_287	scaffold_5	2595029	2596462	-
LINE-20_ML_288	scaffold_5	2596676	2598827	-
Tc1Mariner-3_ML_289	scaffold_5	2638987	2640648	-
RChelitron-1_ML_290	scaffold_5	2652066	2658188	-
Gypsy-6_ML_291	scaffold_5	2709451	2714010	-
Tc1Mariner-1_ML_292	scaffold_5	2719174	2720820	+
LINE-10_ML_293	scaffold_5	2814226	2815648	+
LINE-21_ML_294	scaffold_5	2960906	2964299	+
PIFharbinger-11_ML_295	scaffold_5	3088851	3089915	-
Tc1Mariner-2_ML_296	scaffold_5	3091517	3093169	+
Tc1Mariner-2_ML_297	scaffold_5	3208138	3209791	-
LINE-21_ML_298	scaffold_5	3212209	3215597	-
Tc1Mariner-3_ML_299	scaffold_5	3359363	3361024	-
GremLINE1-1_ML_300	scaffold_5	3401993	3403514	-

Name	Scaffold	Start	End	Strand
GremLINE1-1_ML_301	scaffold_5	3404199	3408900	+
GremLINE1-1_ML_302	scaffold_5	3408903	3414868	+
GremLINE1-1_ML_303	scaffold_5	3414883	3420759	+
GremLINE1-1_ML_304	scaffold_5	3420758	3426676	+
PIFharbinger-11_ML_305	scaffold_6	189507	190584	-
Gypsy-27_ML_306	scaffold_6	261456	262131	-
Tc1Mariner-2_ML_307	scaffold_6	484064	485718	+
LINE-L1-1_ML_308	scaffold_6	798979	801413	+
Gypsy-10_ML_309	scaffold_6	818480	819333	+
Gypsy-10_ML_310	scaffold_6	821986	822839	-
Piggybac-1_Mcir_311	scaffold_6	825490	826708	+
Gypsy-5_ML_312	scaffold_6	1201703	1207692	+
LINE-L1-1_ML_313	scaffold_6	1261081	1262188	-
Tc1Mariner-2_ML_314	scaffold_6	1295554	1297207	+
Tc1Mariner-1_ML_315	scaffold_6	1301159	1302808	-
Tc1Mariner-1_ML_316	scaffold_6	1398415	1400061	+
RChelitron-1_ML_317	scaffold_6	1476610	1478314	+
Gypsy-3_ML_318	scaffold_6	1480244	1486171	+
Tc1Mariner-2_ML_319	scaffold_6	1497219	1498723	+
Gypsy-6_ML_320	scaffold_6	1500247	1504806	+
Tc1Mariner-1_ML_321	scaffold_6	1623151	1624799	-
Tc1Mariner-1_ML_322	scaffold_6	1627994	1629640	+
Gypsy-10_ML_323	scaffold_6	1705645	1706260	+
Gypsy-9_ML_324	scaffold_6	2087868	2090076	+
Tc1Mariner-2_ML_325	scaffold_6	2323793	2325446	+
Gypsy-10_ML_326	scaffold_6	2834217	2835073	+
LINE-L1-4.1_ML_327	scaffold_6	2862505	2863720	+
RChelitron-1_ML_328	scaffold_6	2952733	2958881	-
Tc1Mariner-1_ML_329	scaffold_6	3012273	3013922	+
Tc1Mariner-2_ML_330	scaffold_6	3025523	3027175	-
Tc1Mariner-1_ML_331	scaffold_6	3076254	3077903	+
Gypsy-1_ML_332	scaffold_6	3112118	3117663	+
GremLINE1-1_ML_333	scaffold_6	3187674	3193633	+
GremLINE1-1_ML_334	scaffold_6	3193649	3199609	+
Tc1Mariner-5_ML_335	scaffold_7	0	1379	-
LINE-L1-3_ML_336	scaffold_7	264447	265025	-
LINE-10_ML_337	scaffold_7	265025	270471	-
LINE-11_ML_338	scaffold_7	389869	391725	+
Gypsy-7_ML_339	scaffold_7	447265	449599	-
Gypsy-3_ML_340	scaffold_7	450169	456096	-
Gypsy-28_ML_341	scaffold_7	459419	462658	+
LTR/Unknown-3_ML_342	scaffold_7	462998	463919	+
LINE-L1-1_ML_343	scaffold_7	625148	627509	+

Name	Scaffold	Start	End	Strand
RChelitron-1_ML_344	scaffold_7	1040083	1051000	-
Gypsy-9_ML_345	scaffold_7	1086990	1092080	-
Tc1Mariner-1_ML_346	scaffold_7	1365099	1366748	+
LINE-22_ML_347	scaffold_7	1367512	1370430	-
Gypsy-2_ML_348	scaffold_7	1376029	1382112	-
Gypsy-29_ML_349	scaffold_7	1477134	1478139	-
Gypsy-8_ML_350	scaffold_7	1834035	1840246	-
Gypsy-5_ML_351	scaffold_7	2176890	2182879	+
Tc1Mariner-4_ML_352	scaffold_7	2219779	2221201	-
Tc1Mariner-1_ML_353	scaffold_7	2286049	2287698	-
LINE-L1-1_ML_354	scaffold_7	2320671	2321794	-
Tc1Mariner-2_ML_355	scaffold_7	2445681	2447333	+
LINE-L1-1_ML_356	scaffold_7	2545528	2546696	-
RChelitron-5_ML_357	scaffold_7	2574282	2579010	+
Tc1Mariner-4_ML_358	scaffold_7	2628287	2629080	+
Tc1Mariner-2_ML_359	scaffold_7	2755486	2757140	+
Gypsy-3_ML_360	scaffold_7	2771143	2777070	-
Tc1Mariner-4_ML_361	scaffold_7	2808421	2809849	-
LINE-11_ML_362	scaffold_7	2851478	2852831	+
LINE-3_ML_363	scaffold_8	46922	49246	-
GremLINE1-1_ML_364	scaffold_8	134056	140018	-
GremLINE1-1_ML_365	scaffold_8	140018	145960	-
GremLINE1-1_ML_366	scaffold_8	145984	151949	-
GremLINE1-2_ML_367	scaffold_8	152588	158554	+
GremLINE1-1_ML_368	scaffold_8	158585	164538	+
GremLINE1-1_ML_369	scaffold_8	164538	170493	+
GremLINE1-1_ML_370	scaffold_8	170494	176430	+
GremLINE1-1_ML_371	scaffold_8	176616	182576	+
LINE-19_ML_372	scaffold_8	472858	478330	+
Gypsy-5_ML_373	scaffold_8	566194	572184	-
Tc1Mariner-1_ML_374	scaffold_8	972839	974488	+
Tc1Mariner-10_ML_375	scaffold_8	1266061	1266745	+
Piggybac-1_Mcir_376	scaffold_8	1345074	1346615	+
PIFharbinger-12_ML_377	scaffold_8	1400011	1401187	+
Gypsy-2_ML_378	scaffold_8	1633311	1639394	-
Gypsy-5_ML_379	scaffold_8	1768307	1774297	-
Tc1Mariner-4_ML_380	scaffold_8	1811043	1812457	-
LTR/Unknown-4_ML_381	scaffold_8	1830370	1831108	+
Tc1Mariner-1_ML_382	scaffold_8	1936921	1938569	-
LINE-L1-1_ML_383	scaffold_8	1974982	1977925	-
Gypsy-4_ML_384	scaffold_9	61737	68233	-
Gypsy-4_ML_385	scaffold_9	69676	75730	+
Gypsy-1_ML_386	scaffold_9	118362	123905	+

Name	Scaffold	Start	End	Strand
Gypsy-10_ML_387	scaffold_9	167279	168127	-
Tc1Mariner-2_ML_388	scaffold_9	301202	302854	+
Gypsy-10_ML_389	scaffold_9	351115	351975	+
PIFharbinger-5_ML_390	scaffold_9	547442	548774	-
Tc1Mariner-2_ML_391	scaffold_9	553986	555639	-
LTR/Unknown-5_ML_392	scaffold_9	710552	711569	-
Tc1Mariner-2_ML_393	scaffold_9	711521	713174	-
RChelitron-2_ML_394	scaffold_9	914572	919818	+
PIFharbinger-3_ML_395	scaffold_9	1139875	1140770	-
Piggybac-1_Mcir_396	scaffold_9	1269073	1271098	+
Gypsy-10_ML_397	scaffold_9	1292831	1293685	+
Tc1Mariner-2_ML_398	scaffold_9	1295750	1297402	+
Tc1Mariner-1_ML_399	scaffold_9	1299841	1301510	+
Tc1Mariner-11_ML_400	scaffold_9	1331458	1332640	-
GremLINE1-4_ML_401	scaffold_9	1336100	1342022	-
GremLINE1-1_ML_402	scaffold_9	1342055	1348020	-
GremLINE1-1_ML_403	scaffold_9	1348702	1350387	+
GremLINE1-1_ML_404	scaffold_9	1350401	1356320	+
Tc1Mariner-1_ML_405	scaffold_9	1357999	1359731	+

[1]Class I, RNA transposons or retrotransposons and Class II or DNA transposon predicted in the *M. lusitanicus* MU402 genome. RNA transposons are classified into three major families: GremLINE1, other non-LTR LINE elements, and LTR Ty3/Gypsy; whereas DNA transposons are classified into: Tc1/Mariner, RC/Helitron, and PIF/Harbinger. Every element copy shows a systematic name comprised of the following fields separated by an underscore: transposon subfamily (family and a number delimited by a dash), the acronym of the species in which it was identified (in most cases ML from *M. lusitanicus*), and a number. In addition, their genomic location (scaffold, start, end, and strand) is displayed.

Table S2. FK506 spontaneous resistant isolates from RNAi-deficient and wild-type strains[1]

Strain	Genetic background	Mutation	Effect	GremLINE orientation	Target site duplication
MC7	*dcl1Δ dcl2Δ*	g.48-138dup 91 bp duplication	Frameshift, premature STOP codon caused by duplication		
MC8	*dcl1Δ dcl2Δ*	g.(-8)ins, 534 bp	Frameshift, premature STOP codon caused by insertion	Forward	ATATTAAACATGGGTG
MC9	*dcl1Δ dcl2Δ*	g.76G>T in splicing site	Splice site mutation caused by transversion		
MC10	*dcl1Δ dcl2Δ*	~12 kb GremLINE insertion	Unknown	Unknown	Unknown
MC11	*dcl1Δ dcl2Δ*	g.457A>C in stop codon (p.X109Y)	Nonstop mutation caused by transversion		
MC12	*dcl1Δ dcl2Δ*	g.337ins, 5951	Frameshift, premature STOP caused by insertion	Forward	ACTCAATTGTCTGTT
MC13	*dcl1Δ dcl2Δ*	g.291-341del 51nt deletion	Splice site mutation caused by transversion		
MC14	*dcl1Δ dcl2Δ*	g.455delT in stop codon (p.X109K)	Nonstop mutation caused by deletion		
MC15	*dcl1Δ dcl2Δ*	g.207C>T (p.Q48X)	Premature STOP caused by transition		
MC16	*dcl1Δ dcl2Δ*	~12 kb GremLINE insertion	Unknown	Unknown	Unknown
MC17	*ago1Δ*	g.244ins 36nt (p.E71X)	Several missense mutations, premature STOP caused by insertion	Reverse	GGTCAAGTCATCAAGGGTT
MC18	*ago1Δ*	g.(-54)ins, 5955 bp	Promoter region	Forward	AACCAAACGTTTTT
MC19	*ago1Δ*	g.324delCTCA (p.T65N, p.R74X)	Frameshift, premature STOP caused by deletion		
MC20	*ago1Δ*	g.374G>C (p.A82P)	Missense mutation caused by transversion		
MC21	*ago1Δ*	g.157delTC (p.L31R, p. G34X)	Frameshift, premature STOP caused by deletion		
MC22	*rdrp2Δ*	g.118delA (p.K18R, p.V23X)	Frameshift, premature STOP caused by deletion		
MC23	*rdrp1Δ*	None, wildtype	Possible epimutant		
MC24	*rdrp1Δ*	None, wildtype	Possible epimutant		
MC25	*rdrp1Δ*	None, wildtype	Possible epimutant		
MC26	*rdrp1Δ*	None, wildtype	Possible epimutant		
MC27	*rdrp1Δ*	None, wildtype	Possible epimutant		
MC28	*rdrp1Δ*	None, wildtype	Possible epimutant		
MC29	*rdrp1Δ*	None, wildtype	Possible epimutant		
MC30	*rdrp1Δ*	None, wildtype	Possible epimutant		
MC31	*rdrp1Δ*	None, wildtype	Possible epimutant		
MC32	*rdrp1Δ*	None, wildtype	Possible epimutant		
MC33	MU402	g.241G>A (p.G59D)	Missense mutation caused by transition		
MC34	MU402	g.341G>T (p.E71X)	Nonsense mutation, premature STOP caused by transversion		
MC35	MU402	g.207C>T (p.Q48X)	Nonsense mutation, premature STOP caused by transition		
MC36	MU402	g.124del 42bp deletion (p.G20_G34del)	Microdeletion		
MC37	MU402	g.357insTGAT (p.Y81X)	Frameshift mutation, premature STOP caused by insertion		
MC38	MU402	g.54delTGACC in intron	Possible epimutant		
MC40	MU402	g.417delC (p.L98X)	Frameshift mutation, premature STOP caused by deletion		

Strain	Genetic background	Mutation	Effect	GremLINE orientation	Target site duplication
MC41	MU402	None, wildtype	Possible epimutant		
MC42	MU402	g.441T>C (p.L104P)	Missense mutation caused by transition		

[1]The table shows systematic strain names, genetic background or genotype before the artificial selection experiment and FK506 exposure, mutations characterized, effect of the mutation, GremLINE1 orientation with respect to *fkbA* in those strains that have insertions, and the target duplication site sequences found.

Table S3. GremLINE1 insertions in canonical RNAi-deficient mutants[1]

Query	Subject	% Id	Ins length	Aln length	Mm	Gap	E-value	Score
***ago1*Δ_GremLINE1_1 (MC17)**	GremLINE1-1_ML_102	100	36	35	0	0	2.77E-14	69.9
	GremLINE1-1_ML_103	100	36	35	0	0	2.77E-14	69.9
	GremLINE1-1_ML_106	100	36	35	0	0	2.77E-14	69.9
	GremLINE1-1_ML_116	100	36	35	0	0	2.77E-14	69.9
	GremLINE1-1_ML_118	100	36	35	0	0	2.77E-14	69.9
	GremLINE1-1_ML_119	100	36	35	0	0	2.77E-14	69.9
	GremLINE1-1_ML_123	100	36	35	0	0	2.77E-14	69.9
	GremLINE1-1_ML_205	100	36	35	0	0	2.77E-14	69.9
	GremLINE1-1_ML_206	100	36	35	0	0	2.77E-14	69.9
	GremLINE1-1_ML_207	100	36	35	0	0	2.77E-14	69.9
	GremLINE1-1_ML_208	100	36	35	0	0	2.77E-14	69.9
	GremLINE1-1_ML_209	100	36	35	0	0	2.77E-14	69.9
	GremLINE1-1_ML_211	100	36	35	0	0	2.77E-14	69.9
	GremLINE1-1_ML_213	100	36	35	0	0	2.77E-14	69.9
	GremLINE1-1_ML_301	100	36	35	0	0	2.77E-14	69.9
	GremLINE1-1_ML_302	100	36	35	0	0	2.77E-14	69.9
	GremLINE1-1_ML_303	100	36	35	0	0	2.77E-14	69.9
	GremLINE1-1_ML_333	100	36	35	0	0	2.77E-14	69.9
	GremLINE1-1_ML_334	100	36	35	0	0	2.77E-14	69.9
	GremLINE1-1_ML_364	100	36	35	0	0	2.77E-14	69.9
	GremLINE1-1_ML_365	100	36	35	0	0	2.77E-14	69.9
	GremLINE1-1_ML_366	100	36	35	0	0	2.77E-14	69.9
	GremLINE1-1_ML_369	100	36	35	0	0	2.77E-14	69.9
	GremLINE1-1_ML_370	100	36	35	0	0	2.77E-14	69.9
	GremLINE1-1_ML_402	100	36	35	0	0	2.77E-14	69.9
	GremLINE1-1_ML_74	100	36	35	0	0	2.77E-14	69.9
	GremLINE1-1_ML_91	100	36	35	0	0	2.77E-14	69.9
	GremLINE1-1_ML_92	100	36	35	0	0	2.77E-14	69.9
	GremLINE1-2_ML_120	100	36	35	0	0	2.77E-14	69.9
	GremLINE1-2_ML_169	100	36	35	0	0	2.77E-14	69.9
	GremLINE1-2_ML_170	100	36	35	0	0	2.77E-14	69.9
	GremLINE1-2_ML_247	100	36	35	0	0	2.77E-14	69.9
	GremLINE1-2_ML_367	100	36	35	0	0	2.77E-14	69.9
	GremLINE1-3_ML_127	100	36	35	0	0	2.77E-14	69.9
	GremLINE1-3_ML_246	100	36	35	0	0	2.77E-14	69.9
	GremLINE1-4_ML_104	100	36	35	0	0	2.77E-14	69.9
	GremLINE1-4_ML_105	100	36	35	0	0	2.77E-14	69.9
	GremLINE1-4_ML_115	100	36	35	0	0	2.77E-14	69.9
	GremLINE1-4_ML_117	100	36	35	0	0	2.77E-14	69.9
	GremLINE1-4_ML_124	100	36	35	0	0	2.77E-14	69.9
	GremLINE1-4_ML_204	100	36	35	0	0	2.77E-14	69.9
	GremLINE1-4_ML_210	100	36	35	0	0	2.77E-14	69.9

Query	Subject	% Id	Ins length	AIn length	Mm	Gap	E-value	Score
***ago1Δ*_GremLINE1_1 (MC17)**	GremLINE1-4_ML_401	100	36	35	0	0	2.77E-14	69.9
	GremLINE1-4_ML_72	100	36	35	0	0	2.77E-14	69.9
	GremLINE1-4_ML_245	97.143	36	35	1	0	6.75E-12	61.9
***ago1Δ*_GremLINE1_2 (MC18)**	GremLINE1-1_ML_366	100	5957	5955	0	0	0	11805
	GremLINE1-1_ML_402	100	5957	5955	0	0	0	11805
	GremLINE1-1_ML_92	100	5957	5955	0	0	0	11805
	GremLINE1-1_ML_74	99.916	5957	5934	5	0	0	11724
	GremLINE1-1_ML_333	99.815	5957	5955	11	0	0	11718
	GremLINE1-1_ML_365	99.865	5957	5934	8	0	0	11700
	GremLINE1-1_ML_370	99.848	5957	5930	9	0	0	11684
	GremLINE1-1_ML_73	99.815	5957	5931	11	0	0	11670
	GremLINE1-1_ML_302	99.144	5957	5955	51	0	0	11401
	GremLINE1-1_ML_334	99.144	5957	5955	51	0	0	11401
	GremLINE1-1_ML_368	99.058	5957	5943	55	1	0	11329
	GremLINE1-1_ML_103	99.04	5957	5937	52	3	0	11297
	GremLINE1-2_ML_169	98.842	5957	5956	66	1	0	11256
	GremLINE1-2_ML_367	98.842	5957	5956	66	1	0	11256
	GremLINE1-1_ML_369	98.858	5957	5953	62	4	0	11234
	GremLINE1-1_ML_205	98.757	5957	5955	74	0	0	11218
	GremLINE1-1_ML_206	98.757	5957	5953	74	0	0	11214
	GremLINE1-1_ML_102	98.804	5957	5934	71	0	0	11200
	GremLINE1-1_ML_119	98.772	5957	5943	72	1	0	11194
	GremLINE1-1_ML_116	98.607	5957	5958	80	1	0	11149
	GremLINE1-2_ML_247	98.683	5957	5922	75	1	0	11117
	GremLINE1-1_ML_364	98.556	5957	5954	83	1	0	11117
	GremLINE1-1_ML_371	98.76	5957	5887	73	0	0	11091
	GremLINE1-1_ML_118	98.568	5957	5937	82	1	0	11091
	GremLINE1-1_ML_303	98.689	5957	5872	73	2	0	11018
	GremLINE1-1_ML_404	98.33	5957	5927	85	1	0	10982
	GremLINE1-1_ML_123	98.721	5957	5941	35	31	0	10949
	GremLINE1-1_ML_211	98.499	5957	5864	87	1	0	10919
	GremLINE1-1_ML_208	98.803	5957	5765	65	2	0	10869
	GremLINE1-1_ML_207	98.768	5957	5761	71	0	0	10857
	GremLINE1-1_ML_212	98.278	5957	5866	97	2	0	10816
	GremLINE1-1_ML_209	98.595	5957	5764	78	1	0	10780
	GremLINE1-1_ML_304	95.999	5957	5948	116	87	0	9283
***dcl1Δdcl2Δ*_GremLINE1_1 (MC8)**	GremLINE1-1_ML_103	100	534	534	0	0	0	1059
	GremLINE1-1_ML_106	99.813	534	534	1	0	0	1051
	GremLINE1-4_ML_105	99.813	534	534	1	0	0	1051
	GremLINE1-1_ML_213	98.876	534	534	6	0	0	1011
	GremLINE1-1_ML_102	98.689	534	534	7	0	0	1003
	GremLINE1-1_ML_116	98.689	534	534	7	0	0	1003

Query	Subject	% Id	Ins length	AIn length	Mm	Gap	E-value	Score
***dcl1Δdcl2Δ*_GremLINE1_1 (MC8)**	GremLINE1-1_ML_209	98.689	534	534	7	0	0	1003
	GremLINE1-1_ML_211	98.689	534	534	7	0	0	1003
	GremLINE1-1_ML_301	98.689	534	534	7	0	0	1003
	GremLINE1-1_ML_302	98.689	534	534	7	0	0	1003
	GremLINE1-1_ML_333	98.689	534	534	7	0	0	1003
	GremLINE1-1_ML_365	98.689	534	534	7	0	0	1003
	GremLINE1-1_ML_366	98.689	534	534	7	0	0	1003
	GremLINE1-1_ML_369	98.689	534	534	7	0	0	1003
	GremLINE1-1_ML_370	98.689	534	534	7	0	0	1003
	GremLINE1-1_ML_402	98.689	534	534	7	0	0	1003
	GremLINE1-1_ML_74	98.689	534	534	7	0	0	1003
	GremLINE1-1_ML_92	98.689	534	534	7	0	0	1003
	GremLINE1-3_ML_246	98.689	534	534	7	0	0	1003
	GremLINE1-4_ML_210	98.689	534	534	7	0	0	1003
	GremLINE1-1_ML_249	98.684	534	532	7	0	0	999
	GremLINE1-1_ML_118	98.502	534	534	8	0	0	995
	GremLINE1-1_ML_364	98.502	534	534	8	0	0	995
	GremLINE1-1_ML_91	98.502	534	534	8	0	0	995
	GremLINE1-4_ML_104	98.502	534	534	8	0	0	995
	GremLINE1-4_ML_117	98.502	534	534	8	0	0	995
	GremLINE1-4_ML_124	98.502	534	534	8	0	0	995
	GremLINE1-4_ML_245	98.502	534	534	8	0	0	995
	GremLINE1-4_ML_401	98.502	534	534	8	0	0	995
	GremLINE1-4_ML_72	98.502	534	534	8	0	0	995
	GremLINE1-1_ML_303	98.496	534	532	8	0	0	991
	GremLINE1-3_ML_127	98.496	534	532	8	0	0	991
	GremLINE1-1_ML_73	98.491	534	530	8	0	0	987
	GremLINE1-4_ML_115	98.315	534	534	9	0	0	987
	GremLINE1-4_ML_204	98.315	534	534	9	0	0	987
	GremLINE1-1_ML_300	98.308	534	532	9	0	0	983
	GremLINE1-4_ML_248	98.124	534	533	10	0	0	977
	GremLINE1-1_ML_368	98.124	534	533	9	1	0	969
	GremLINE1-1_ML_212	97.932	534	532	11	0	0	967
	GremLINE1-1_ML_119	97.753	534	534	12	0	0	963
	GremLINE1-2_ML_120	97.753	534	534	12	0	0	963
	GremLINE1-2_ML_169	97.753	534	534	12	0	0	963
	GremLINE1-2_ML_247	97.753	534	534	12	0	0	963
	GremLINE1-2_ML_367	97.753	534	534	12	0	0	963
	GremLINE1-1_ML_206	97.378	534	534	14	0	0	948
	GremLINE1-1_ML_207	97.378	534	534	14	0	0	948
	GremLINE1-1_ML_208	97.378	534	534	14	0	0	948
	GremLINE1-1_ML_403	97.368	534	532	14	0	0	944
	GremLINE1-1_ML_334	97.191	534	534	15	0	0	940

Query	Subject	% Id	Ins length	Aln length	Mm	Gap	E-value	Score
***dcl1Δdcl2Δ*_GremLINE1_1 (MC8)**	GremLINE1-1_ML_123	97.575	534	536	7	4	0	932
	GremLINE1-1_ML_205	96.816	534	534	17	0	0	924
	GremLINE1-2_ML_170	96.816	534	534	17	0	0	924
	GremLINE1-1_ML_304	96.84	534	538	11	5	0	894
	GremLINE1-1_ML_404	95.113	534	532	12	1	0	866
	GremLINE1-1_ML_371	93.843	534	536	31	1	0	795
	GremLINE1-5_ML_250	93.084	534	535	31	3	0	749
***dcl1Δdcl2Δ*_GremLINE1_3 (MC12)**	GremLINE1-1_ML_366	99.95	5951	5951	3	0	0	11773
	GremLINE1-1_ML_402	99.95	5951	5951	3	0	0	11773
	GremLINE1-1_ML_92	99.95	5951	5950	3	0	0	11771
	GremLINE1-1_ML_74	99.865	5951	5939	8	0	0	11710
	GremLINE1-1_ML_365	99.815	5951	5938	11	0	0	11684
	GremLINE1-1_ML_333	99.765	5951	5950	14	0	0	11684
	GremLINE1-1_ML_370	99.798	5951	5935	12	0	0	11670
	GremLINE1-1_ML_73	99.764	5951	5931	14	0	0	11646
	GremLINE1-1_ML_302	99.093	5951	5951	54	0	0	11369
	GremLINE1-1_ML_334	99.093	5951	5951	54	0	0	11369
	GremLINE1-1_ML_368	99.007	5951	5943	58	1	0	11305
	GremLINE1-1_ML_103	98.99	5951	5942	55	3	0	11284
	GremLINE1-2_ML_169	98.791	5951	5954	69	1	0	11228
	GremLINE1-2_ML_367	98.791	5951	5954	69	1	0	11228
	GremLINE1-1_ML_369	98.808	5951	5954	65	4	0	11212
	GremLINE1-1_ML_205	98.706	5951	5951	77	0	0	11186
	GremLINE1-1_ML_206	98.706	5951	5951	77	0	0	11186
	GremLINE1-1_ML_102	98.753	5951	5935	74	0	0	11178
	GremLINE1-1_ML_119	98.721	5951	5944	75	1	0	11173
	GremLINE1-1_ML_116	98.556	5951	5954	83	1	0	11117
	GremLINE1-2_ML_247	98.633	5951	5927	78	1	0	11103
	GremLINE1-1_ML_364	98.505	5951	5954	86	1	0	11093
	GremLINE1-1_ML_118	98.519	5951	5940	85	1	0	11073
	GremLINE1-1_ML_371	98.74	5951	5873	74	0	0	11056
	GremLINE1-1_ML_303	98.639	5951	5877	76	2	0	11004
	GremLINE1-1_ML_404	98.279	5951	5927	88	1	0	10958
	GremLINE1-1_ML_123	98.671	5951	5943	38	31	0	10929
	GremLINE1-1_ML_211	98.449	5951	5869	90	1	0	10905
	GremLINE1-1_ML_208	98.752	5951	5770	68	2	0	10855
	GremLINE1-1_ML_207	98.717	5951	5766	74	0	0	10843
	GremLINE1-1_ML_212	98.227	5951	5866	100	2	0	10792
	GremLINE1-1_ML_209	98.543	5951	5767	81	1	0	10762
	GremLINE1-1_ML_304	95.948	5951	5948	119	87	0	9260

[1]The table shows whole insertion sequence (query) BLASTn hits against a nucleotide database containing every TE element sequence in the genome (subject). In addition, percentage of identity (% Id), whole length of the insertion (ins length) and the BLAST alignment (aln length), number of mismatches

(mm) or gaps (gap) in the alignment, and BLAST e-value and score are depicted. BLAST hits whose alignment length was < 97% of the query sequence were filtered out to ensure hits corresponding to most of the inserted sequence, and the remaining hits (alignment length ≥ 97% of the query sequence) are sorted by highest score, lowest e-value, and highest BLAST alignment length, in that order. Light green shading indicates the best scoring and longest alignments for each query.

Table S4. Primers used in this study[1]

Name	Sequence	Description
JOHE51492	aagagagtctcgtctcgtctcctggtgactggtgaTGCCTCAGCATTGGTACTTG	*clr4* deletion, overlap with *pyrG*
JOHE51493	atgcattagatcctcactcggagacacggccaatgGTACACTGGCCATGCTATCG	*clr4* deletion, overlap with *pyrG*
JOHE51682	CAGCGGTTTGGTTGAATGCC	*clr4* deletion
JOHE51604	TCCTCCTCCGCAACAACAAC	*clr4* deletion
JOHE52150	GCGAAACGAACTCAGTCATGG	*clr4* deletion, WT allele PCR
JOHE52151	TGTGCCTTTGGGAATGTCTTG	*clr4* deletion, WT allele PCR
JOHE51684	GGAGCTTGGTGAGGGTTAGC	*clr4* deletion, 3´spanning MUT allele PCR
JOHE51510	CCTTTGTTTGTGTGCTCAAGGT	*clr4* deletion, 3´spanning MUT allele PCR
JOHE51718	GTCTTGTCTCATGCAGACT	GremLINE1 qPCR
JOHE51719	GCACCAAGAGAGAGACGAGC	GremLINE1 qPCR
JOHE51666	CAGCACCAACAACAGTGACG	*vma1* qPCR
JOHE51668	ACCTTGGTGCTCGTCTTGCC	*vma1* qPCR
JOHE52223	AATCGCAACGGAATTCCTGACCGGAC	*fkbA* amplification and Sanger sequencing
JOHE52224	CTCAAGACGGACGAGCCTCA	*fkbA* amplification and Sanger sequencing
JOHE51780	AAAACGCGAAACAGCAAACG	*fkbA* Sanger sequencing
JOHE51782	AGGCTACCTTGAACTTTGAAG	*fkbA* Sanger sequencing
JOHE52501	TTGGTGATCGTGTGGATGC	TE insertion Sanger sequencing
JOHE52502	GTTACACCAAGAAGCAGAAGG	TE insertion Sanger sequencing
JOHE52503	TCTGGTGTTTCTGGCTCTGG	TE insertion Sanger sequencing
JOHE52504	GCTAGTATTGGTCCTGGTAGT	TE insertion Sanger sequencing
JOHE52505	GATGGTGATATGCTGACGGCA	TE insertion Sanger sequencing
JOHE52506	GGCGTTTGAGCCTTTGCTTC	TE insertion Sanger sequencing
JOHE52507	CCTTGGTTCTCTTTCCCTGAG	TE insertion Sanger sequencing
JOHE52508	TGGCTATGAACATGAGTGTGG	TE insertion Sanger sequencing
JOHE52509	CACTCGTTGGCTCGAACAGG	TE insertion Sanger sequencing
JOHE52510	GGCTAACTCGTTACTGTTGTCC	TE insertion Sanger sequencing
JOHE52582	CCACACTCATGTTCATAGCCACA	TE insertion Sanger sequencing
JOHE52583	CCTGTTCGAGCCAACGAGTG	TE insertion Sanger sequencing
JOHE52584	GGACAACAGTAACGAGTTAGCC	TE insertion Sanger sequencing
JOHE52585	CTCATCATAGACGCTCAAAGGC	TE insertion Sanger sequencing
JOHE52586	GCTACTCGTTCTTGGTGCTATG	TE insertion Sanger sequencing

[1]Every primer shows systematic name, nucleotide sequence (in 5'-3' direction), and a brief description explaining its use. Lowercase nucleotides overlap with the *pyrG* marker for *clr4* deletion.

Dataset S1 (separate file). RNA interference (RNAi) components, histone-lysine (KMT) and DNA 5mC methyltransferases (DNMT), and histone demethylases (KDM) in fungi. Homologs of RNAi components and chromatin modifying enzymes (left, Protein) identified in each given species (Species, and Source for genome references). Each identified homolog (Subject) shows PSI-BLAST percentage of identity (% Id), E-value, score, and its matching query sequence (Query). Next, percentage of identity, E-value, and score of a reciprocal BLAST against that same query (Recip). For every homolog, protein length, InterPro protein domains (IPR and Description), their start and end positions, and their prediction E-value is also shown. Subjects (identified homologs) from JGI/Broad Institute show a JGI protein ID (or FungiDB gene ID if available), whereas those from *Absidia glauca* show an Ensembl gene ID. Queries (and reciprocal hits) show their species name as a three-letter abbreviation (or four-letter for disambiguation, first letter from their genus and two/three first letters from their species epithet), the protein name, and their identifier separated by an underscore. For both subjects and queries, known and experimentally curated IDs may show their gene name/symbol at the end after a dash character.

Dataset S2 (separate file). Fungal RNAi, KMT, DNMT, and KDM enzyme protein domain architecture. Full-length, scaled protein sequences of every identified protein homologs and their predicted, color-coded protein domains (rectangles) are shown. Identified homologs from JGI/Broad Institute show a JGI protein ID (or FungiDB gene ID if available), whereas those from *Absidia glauca* show an Ensembl gene ID, and experimentally curated proteins may show their gene name/symbol instead of their ID.

Dataset S3 (separate file). Major transposable element families and subfamilies, their ORFs, and protein domain configurations. The full-length, scaled nucleotide sequences of the major transposable element families and subfamilies identified in M. lusitanicus are depicted. Each family shows ORF prediction (gray arrowed blocks), as well as encoded InterPro protein domains (color-coded rectangles).

Dataset S4 (separate file). Fungal RNAi, KMT, DNMT, and KDM enzyme protein FASTA sequences.

SI References

85. C. Camacho, *et al.*, BLAST+: architecture and applications. *BMC Bioinformatics* **10**, 421 (2009).

86. A. Goffeau, *et al.*, Life with 6000 genes. *Science* **274**, 546–567 (1996).

87. J. E. Galagan, *et al.*, The genome sequence of the filamentous fungus *Neurospora crassa*. *Nature* **422**, 859–868 (2003).

88. N. Rhind, *et al.*, Comparative functional genomics of the fission yeasts. *Science* **332**, 930–936 (2011).

89. Å. Olson, *et al.*, Insight into trade-off between wood decay and parasitism from the genome of a fungal forest pathogen. *New Phytol.* **194**, 1001–1013 (2012).

90. T. Y. James, *et al.*, Shared signatures of parasitism and phylogenomics unite Cryptomycota and Microsporidia. *Curr. Biol.* **23**, 1548–1553 (2013).

91. S. Ellenberger, A. Burmester, J. Wöstemeyer, Complete mitochondrial DNA sequence of the Mucoralean fusion parasite *Parasitella parasitica*. *Genome Announc.* **2**, e00912-14 (2014).

92. J. Linde, *et al.*, De novo whole-genome sequence and genome annotation of *Lichtheimia ramosa*. *Genome Announc.* **2**, e00888-14 (2014).

93. V. U. Schwartze, *et al.*, Gene expansion shapes genome architecture in the human pathogen *Lichtheimia corymbifera*: an evolutionary genomics analysis in the ancient terrestrial Mucorales (Mucoromycotina). *PLoS Genet.* **10**, e1004496 (2014).

94. S. Triana, *et al.*, Draft genome sequence of the animal and human pathogen *Malassezia pachydermatis* strain CBS 1879. *Genome Announc.* **3**, e01197-15 (2015).

95. S. Ellenberger, A. Burmester, J. Wöstemeyer, Complete mitochondrial DNA sequence of the Mucoralean fungus *Absidia glauca*, a model for studying host-parasite interactions. *Genome Announc.* **4**, e00153-16 (2016).

96. F. Rabe, *et al.*, A complete toolset for the study of *Ustilago bromivora* and *Brachypodium* sp. as a fungal-temperate grass pathosystem. *eLife* **5**, e20522 (2016).

97. C. Russ, *et al.*, Genome sequence of *Spizellomyces punctatus*. *Genome Announc.* **4**, e00849-16 (2016).

98. T. Jones, *et al.*, The diploid genome sequence of *Candida albicans*. *Proc. Natl. Acad. Sci. U. S. A.* **101**, 7329–7334 (2004).

99. C. A. Cuomo, *et al.*, Comparative analysis highlights variable genome content of wheat rusts and divergence of the mating loci. *G3 Genes|Genomes|Genetics* **7**, 361–376 (2017).

100. S. R. Lockhart, *et al.*, Simultaneous emergence of multidrug-resistant *Candida auris* on 3 continents confirmed by whole-genome sequencing and epidemiological analyses. *Clin. Infect. Dis.* **64**, 134–140 (2017).

101. C. A. Quandt, *et al.*, The genome of an intranuclear parasite, *Paramicrosporidium saccamoebae*, reveals alternative adaptations to obligate intracellular parasitism. *eLife* **6**, e29594 (2017).

102. J. Uehling, *et al.*, Comparative genomics of *Mortierella elongata* and its bacterial endosymbiont *Mycoavidus cysteinexigens*. *Environ. Microbiol.* **19**, 2964–2983 (2017).

103. E. C. H. Chen, *et al.*, High intraspecific genome diversity in the model arbuscular mycorrhizal symbiont *Rhizophagus irregularis*. *New Phytol.* **220**, 1161–1171 (2018).

104. Y. Kobayashi, *et al.*, The genome of *Rhizophagus clarus* HR1 reveals a common genetic

basis for auxotrophy among arbuscular mycorrhizal fungi. *BMC Genomics* **19**, 465 (2018).

105. Y. Chang, *et al.*, Phylogenomics of Endogonaceae and evolution of mycorrhizas within Mucoromycota. *New Phytol.* **222**, 511–525 (2019).

106. E. Morin, *et al.*, Comparative genomics of *Rhizophagus irregularis*, *R. cerebriforme*, *R. diaphanus* and *Gigaspora rosea* highlights specific genetic features in Glomeromycotina. *New Phytol.* **222**, 1584–1598 (2019).

107. F. Venice, *et al.*, At the nexus of three kingdoms: the genome of the mycorrhizal fungus *Gigaspora margarita* provides insights into plant, endobacterial and fungal interactions. *Environ. Microbiol.* **22**, 122–141 (2020).

108. B. Wang, *et al.*, Chromosome-scale genome assembly of *Fusarium oxysporum* strain Fo47, a fungal endophyte and biocontrol Agent. *Mol. Plant-Microbe Interact.* **33**, 1108–1111 (2020).

109. R. A. Dean, *et al.*, The genome sequence of the rice blast fungus *Magnaporthe grisea*. *Nature* **434**, 980–986 (2005).

110. Y. Chang, *et al.*, Genome-scale phylogenetic analyses confirm *Olpidium* as the closest living zoosporic fungus to the non-flagellated, terrestrial fungi. *Sci. Rep.* **11**, 3217 (2021).

111. M. Malar C, *et al.*, The genome of *Geosiphon pyriformis* reveals ancestral traits linked to the emergence of the arbuscular mycorrhizal symbiosis. *Curr. Biol.* **31**, 1570-1577.e4 (2021).

112. K. R. Amses, *et al.*, Diploid-dominant life cycles characterize the early evolution of Fungi. *Proc. Natl. Acad. Sci. U. S. A.* **119**, e2116841119 (2022).

113. Y. Chang, *et al.*, Evolution of zygomycete secretomes and the origins of terrestrial fungal

ecologies. *iScience* **25**, 104840 (2022).

114. W. C. Nierman, *et al.*, Genomic sequence of the pathogenic and allergenic filamentous fungus *Aspergillus fumigatus*. *Nature* **438**, 1151–1156 (2005).

115. J. Kämper, *et al.*, Insights from the genome of the biotrophic fungal plant pathogen *Ustilago maydis*. *Nature* **444**, 97–101 (2006).

116. C. A. Cuomo, *et al.*, The *Fusarium graminearum* genome reveals a link between localized polymorphism and pathogen specialization. *Science* **317**, 1400–1402 (2007).

117. T. J. Sharpton, *et al.*, Comparative genomic analyses of the human fungal pathogens *Coccidioides* and their relatives. *Genome Res.* **19**, 1722–1731 (2009).

118. N. Corradi, J.-F. Pombert, L. Farinelli, E. S. Didier, P. J. Keeling, The complete sequence of the smallest known nuclear genome from the microsporidian *Encephalitozoon intestinalis*. *Nat. Commun.* **1**, 77 (2010).

119. S. B. Goodwin, *et al.*, Finished genome of the fungal wheat pathogen *Mycosphaerella graminicola* reveals dispensome structure, chromosome plasticity, and stealth pathogenesis. *PLoS Genet.* **7**, e1002070 (2011).

120. P. Jones, *et al.*, InterProScan 5: genome-scale protein function classification. *Bioinformatics* **30**, 1236–1240 (2014).

121. M. Manni, M. R. Berkeley, M. Seppey, F. A. Simão, E. M. Zdobnov, BUSCO update: novel and streamlined workflows along with broader and deeper phylogenetic coverage for scoring of eukaryotic, prokaryotic, and viral genomes. *Mol. Biol. Evol.* **38**, 4647–4654 (2021).

122. K. Katoh, D. M. Standley, MAFFT multiple sequence alignment software version 7: improvements in performance and usability. *Mol. Biol. Evol.* **30**, 772–780 (2013).

123. S. Capella-Gutierrez, J. M. Silla-Martinez, T. Gabaldon, trimAl: a tool for automated alignment trimming in large-scale phylogenetic analyses. *Bioinformatics* **25**, 1972–1973 (2009).

124. B. Q. Minh, *et al.*, IQ-TREE 2: new models and efficient methods for phylogenetic inference in the genomic era. *Mol. Biol. Evol.* **37**, 1530–1534 (2020).

125. J. M. Flynn, *et al.*, RepeatModeler2 for automated genomic discovery of transposable element families. *Proc. Natl. Acad. Sci. U. S. A.* **117**, 9451–9457 (2020).

126. W. Bao, K. K. Kojima, O. Kohany, Repbase Update, a database of repetitive elements in eukaryotic genomes. *Mob. DNA* **6**, 11 (2015).

127. P. Rice, I. Longden, A. Bleasby, EMBOSS: the European Molecular Biology Open Software Suite. *Trends Genet.* **16**, 276–7 (2000).

128. C. Llorens, *et al.*, The Gypsy Database (GyDB) of mobile genetic elements: release 2.0. *Nucleic Acids Res.* **39**, D70–D74 (2011).

129. P. Ewels, M. Magnusson, S. Lundin, M. Käller, MultiQC: summarize analysis results for multiple tools and samples in a single report. *Bioinformatics* **32**, 3047–3048 (2016).

130. M. Martin, Cutadapt removes adapter sequences from high-throughput sequencing reads. *EMBnet.journal* **17**, 10–12 (2011).

131. H. Li, *et al.*, The Sequence Alignment/Map format and SAMtools. *Bioinformatics* **25**, 2078–2079 (2009).

132. F. Ramírez, *et al.*, deepTools2: a next generation web server for deep-sequencing data analysis. *Nucleic Acids Res.* **44**, W160–W165 (2016).

133. Y. Zhang, *et al.*, Model-based Analysis of ChIP-Seq (MACS). *Genome Biol.* **9**, R137

(2008).

134. W. J. Kent, A. S. Zweig, G. Barber, A. S. Hinrichs, D. Karolchik, BigWig and BigBed: enabling browsing of large distributed datasets. *Bioinformatics* **26**, 2204–2207 (2010).

135. A. R. Quinlan, I. M. Hall, BEDTools: a flexible suite of utilities for comparing genomic features. *Bioinformatics* **26**, 841–842 (2010).

136. A. Dobin, T. R. Gingeras, “Mapping RNA-seq Reads with STAR” in *Current Protocols in Bioinformatics*, (John Wiley & Sons, Inc., 2015), pp. 11.14.1-11.14.19.

137. Y. Liao, G. K. Smyth, W. Shi, featureCounts: an efficient general purpose program for assigning sequence reads to genomic features. *Bioinformatics* **30**, 923–930 (2014).

138. M. E. Ritchie, *et al.*, limma powers differential expression analyses for RNA-sequencing and microarray studies. *Nucleic Acids Res.* **43**, e47–e47 (2015).

139. T. Smith, A. Heger, I. Sudbery, UMI-tools: modeling sequencing errors in Unique Molecular Identifiers to improve quantification accuracy. *Genome Res.* **27**, 491–499 (2017).

140. B. Langmead, C. Trapnell, M. Pop, S. L. Salzberg, Ultrafast and memory-efficient alignment of short DNA sequences to the human genome. *Genome Biol.* **10**, R25 (2009).

141. P. P. Chan, B. Y. Lin, A. J. Mak, T. M. Lowe, tRNAscan-SE 2.0: improved detection and functional classification of transfer RNA genes. *Nucleic Acids Res.* **49**, 9077–9096 (2021).

142. M. J. Axtell, ShortStack: Comprehensive annotation and quantification of small RNA genes. *RNA* **19**, 740–751 (2013).

143. H. Wickham, *ggplot2* (Springer New York, 2009) https:/doi.org/10.1007/978-0-387-98141-

3.

144. T. Hothorn, F. Bretz, P. Westfall, Simultaneous inference in general parametric models. *Biometrical J.* **50**, 346–363 (2008).

145. L. Lopez-Delisle, *et al.*, pyGenomeTracks: reproducible plots for multivariate genomic datasets. *Bioinformatics* **37**, 422–423 (2021).

146. E. Paradis, K. Schliep, ape 5.0: an environment for modern phylogenetics and evolutionary analyses in R. *Bioinformatics* **35**, 526–528 (2019).